Supplementary Information

1 Detailed Methods

The all-silica zeolites frameworks were selected from the 110 orthogonal structures in the International Zeolite Association (IZA) database[1] and the orthogonal structures in the predicted crystallography open database (PCOD)[2]. The PCOD database[2] was reduced to a set of 121,966 structures by removing those with a largest free-sphere diameter below 2.25 Å as these are less accessible to carbon dioxide (CO_2) (Figs. S13–S14); of these, a randomly chosen subset of 81,526 structures was screened. Note that some of the results for the IZA zeolites appear outside the range of the hypothetical zeolite results, which may be due to the energy minimization step used in the construction of the hypothetical zeolite database.[2] The geometric structure descriptors of largest included sphere diameter, largest free sphere diameter, and accessible surface area was obtained using the open-source software Zeo++,[3] using its high accuracy setting,[4], a methane (CH_4) probe of 1.625 Å radius, a silicon atom radius of 2.10 Å, and an oxygen atom radius of 1.52 Å.

Mixture adsorption isotherms were produced both directly by grand-canonical Monte Carlo (GCMC) simulation[5] and from the simulated pure-component isotherms using Ideal Adsorbed Solution Theory (IAST).[6] Except for where the two results were compared, the directly-generated mixture isotherms were used throughout this paper. All isotherms were generated with a GPU GCMC code that has been described elsewhere,[7,8] which uses a parallel flood fill algorithm to find blocked pockets inaccessible from the gas phase[7] and uses density-biased sampling to accelerate convergence.[8] The force field developed by García-Pérez *et al.*[9] was used, which consists of Lennard-Jones and Coulombic terms for guest-guest and guest-host interactions. The host framework atoms were assumed to be rigid, and the number of simulated unit cells was chosen such that the simulation box extended at least twice the cutoff radius of 12 Å. Our work exclusively used units of absolute loading.

To directly generate mixture isotherms, the GPU GCMC code was adapted to allow for multiple adsorbate species, and blocked pockets were separately found and applied to CH_4 and CO_2. For all zeolites, the number of equilibration and production steps, respectively, were set to 10,000,000 and 1,000,000 for the associated petrolum gas (APG) and non-associated gas (NAG) processes for which isotherms were simulated up to 100 bar, and 5,000,000 and 1,000,000 for the landfill gas (LFG) process for which isotherms were simulated up to 5 bar. These numbers of steps were validated as being sufficient for isotherm convergence[8] at the pressures involved for screening the three processes studied in this paper by comparison to isotherms created using a conventional CPU-based code (Figs. S24–S29).

To generate mixture isotherms by IAST, pure-component isotherms for the IZA zeolites were generated using 5,000,000 equilibration and 3,000,000 production steps, pure-component isotherms for the hypothetical zeolites with a largest free-sphere diameter less than 3.75 Å were generated using 1,250,000 equilibration and 500,000 production steps, and pure-component isotherms for the hypothetical zeolites with a largest free-sphere diameter greater than 3.75 Å were taken from previous work.[10,11] The number of steps used to generate pure-component isotherms for the hypothetical zeolites with a largest free-sphere diameter less than 3.75 Å were chosen to achieve a similar degree of convergence as the pure-component isotherms taken from previous work. The pure-component isotherms were then fit via the method of least squares to single- or dual-site Langmuir isotherms for each adsorbate based on which fit gave a larger adjusted R^2 value for that adsorbate. The spreading pressure was then calculated via analytical integration of equation 19 of Myers and Prausnitz[6]. As this procedure sometimes requires the fitted isotherms to be evaluated at pressures above the highest pressure point of the simulated isotherms, we only allowed such extrapolation for structures which had fitted saturation loading capacities less than ten times the amount of the loading at the highest simulated pressure

point; the remainder were not used in comparing IAST results to directly-generated mixture isotherm results. The fitted saturation loading capacities of these pure-component adsorption isotherms were used in plots in this paper as stated (fitted Henry coefficients were not used in plots as we instead used values obtained from Widom insertions; see below). When a dual-site Langmuir isotherm was used, the sum of the two saturation loading capacities was used.

The Peng-Robinson equation of state[12] was used to convert between pressure and fugacity, with the critical temperatures, critical pressures, and acentric factors of CH_4 and CO_2 being 190.6 K, 46.0 bar, 0.008, 304.2 K, 73.76 bar, and 0.225, respectively. For mixture isotherms generated directly by GCMC, the known total pressure and mole fractions were converted to component fugacities using the van der Waals mixing rules with a binary interaction parameter of 0.0919, which were then used as inputs to the simulations. For pure-component isotherms used for IAST, the component's fugacity was input directly to the simulation and then converted to pressure prior to IAST calculations; however, in Fig. 8 fugacity was not converted to pressure prior to the IAST calculation to ensure consistency of units on the x-axis.

Widom insertions were performed by the GPU code[7,8] to calculate isosteric heats of adsorption, Henry coefficients, and helium void fractions, all at 300 K. Some zeolites have no enthalpically favorable adsorption sites for CH_4, either intrinsically or due to blocking; $Q_{\mathrm{st,CH_4}}$ for these materials was set to $0\,\mathrm{kJ\,mol^{-1}}$ for the purposes of plotting and for calculating the objective function. Isosteric heats of adsorption and Henry coefficients for all materials were calculated using 200,000 Widom insertions. For all materials, helium void fractions were calculated using 100,000 Widom insertions and the force field of Talu and Myers[13].

As different materials perform optimally at different conditions, we evaluated each material at its own optimal desorption conditions to allow for fair comparison. For each zeolite, the optimal desorption pressure (PSA), temperature (TSA), or both (PTSA) was found by minimization of the objective function value (OFV). We note that future studies may need not strictly find each adsorbent's optimal desorption conditions if desorption conditions can be well-approximated prior to the study's commencement, as we found that the Separation Performance Parameters (SPP values) for the adsorbents undergoing the three PSA processes at set desorption pressures are well-correlated with the SPP values for the adsorbents undergoing the three PSA processes at each adsorbent's optimal desorption pressure (Fig. S30). For our study, we used the optimal desorption conditions for all analyses except for the data presented in Fig. S30 and for the comparison of the various metrics presented in Figs. 1 and S1, since we found that the Sorbent Selection Parameter and Adsorbent Performance Indicator could not be used to find the optimal desorption conditions. SciPy version 0.15.1 was used to perform the minimization.[14] The adsorption pressures were set by the process, and the adsorption temperature was always 300 K. The desorption temperature was constrained to be greater than or equal to 300 K for TSA and PTSA and set to 300 K for PSA, while the desorption pressure was constrained to be between 0.1 bar and 1 bar for PSA and PTSA and set to 1 bar for TSA. The mole fractions were set by the process, and the same mole fraction was used for both adsorption and desorption. For all materials, mixture isotherms generated at 300 K were used, and for the IZA zeolites, upon which TSA and PTSA were also performed, mixture isotherms were also generated at higher temperatures going up in 5 K increments. Continuous optimization was applied to find the optimal desorption pressure, applying Akima cubic spline interpolation[15] as implemented by SciPy[14] to calculate loadings between the pressures that were simulated. Discrete optimization was applied to find the optimal desorption temperature in 5 K increments. For PTSA, pressure optimization was performed for all desorption temperatures, and the temperature that gave the lowest OFV was then chosen. When mixture isotherms gave a negative working capacity for either adsorbate (possible since mixture isotherms are not necessarily monotonically increasing functions), the working capacity for that adsorbate was set to $0\,\mathrm{mol\,kg^{-1}}$ prior to calculation of the metrics that go into the objective function.

To implement the random forest of decision trees regression algorithm and calculate the importances of the individual descriptors, we used open-source scikit-learn version 0.14.1-2.[16] Our forest included 1,000 trees, which has been shown to be an adequate number for random forest accuracy.[17] Nodes were expanded until all leaves were pure.

We have placed the computer code we developed for the screening online with the Open Science Framework, along with the pure and mixture isotherms and the screening results.[18] The code is capable of computing the SPP, Sorbent Selection Parameter, or Adsorbent Performance Indicator at optimized or set

desorption conditions. Mixture isotherms can be input directly as loadings at multiple pressures, in which case the code will perform interpolation to calculate loadings, or mixture isotherms will be calculated by the code using IAST with pure-component isotherms input either as loadings at multiple pressures or as already-fitted dual-site Langmuir isotherms.

2 Derivation of Metrics

The derivation of the terms in the SPP begins by calculating the mole fraction of CH_4 in the raffinate stream:

$$\begin{aligned} y_{\mathrm{CH_4,raff}} &= \frac{M_{\mathrm{CH_4,raff}}}{M_{\mathrm{CH_4,raff}} + M_{\mathrm{CO_2,raff}}} \\ &= \frac{M_{\mathrm{CH_4,feed}} - \Delta q_{\mathrm{CH_4}} M_{\mathrm{ads}}}{(M_{\mathrm{CH_4,feed}} - \Delta q_{\mathrm{CH_4}} M_{\mathrm{ads}}) + (M_{\mathrm{CO_2,feed}} - \Delta q_{\mathrm{CO_2}} M_{\mathrm{ads}})} \\ &= \frac{1 - \Delta q_{\mathrm{CH_4}} \frac{M_{\mathrm{ads}}}{M_{\mathrm{CH_4,feed}}}}{(1 - \Delta q_{\mathrm{CH_4}} \frac{M_{\mathrm{ads}}}{M_{\mathrm{CH_4,feed}}}) + (\frac{y_{\mathrm{CO_2,feed}}}{y_{\mathrm{CH_4,feed}}} - \Delta q_{\mathrm{CO_2}} \frac{M_{\mathrm{ads}}}{M_{\mathrm{CH_4,feed}}})} \\ &= \frac{1 - \Delta q_{\mathrm{CH_4}} \frac{M_{\mathrm{ads}}}{M_{\mathrm{CH_4,feed}}}}{\frac{1}{y_{\mathrm{CH_4,feed}}} - \frac{M_{\mathrm{ads}}}{M_{\mathrm{CH_4,feed}}} (\Delta q_{\mathrm{CH_4}} + \Delta q_{\mathrm{CO_2}})} \end{aligned}$$

Rearranging, we obtain:

$$\frac{M_{\mathrm{ads}}}{M_{\mathrm{CH_4,feed}}} = \frac{y_{\mathrm{CH_4,raff}} - y_{\mathrm{CH_4,feed}}}{y_{\mathrm{CH_4,feed}} \left[y_{\mathrm{CH_4,raff}} \left(\Delta q_{\mathrm{CH_4}} + \Delta q_{\mathrm{CO_2}} \right) - \Delta q_{\mathrm{CH_4}} \right]} \tag{1}$$

We then calculate the moles of recovered CH_4 per moles of feed CH_4:

$$\begin{aligned} \frac{M_{\mathrm{CH_4,raff}}}{M_{\mathrm{CH_4,feed}}} &= \frac{M_{\mathrm{CH_4,feed}} - \Delta q_{\mathrm{CH_4}} M_{\mathrm{ads}}}{M_{\mathrm{CH_4,feed}}} \\ &= 1 - \Delta q_{\mathrm{CH_4}} \frac{M_{\mathrm{ads}}}{M_{\mathrm{CH_4,feed}}} \\ &= 1 - \Delta q_{\mathrm{CH_4}} \left(\frac{y_{\mathrm{CH_4,raff}} - y_{\mathrm{CH_4,feed}}}{y_{\mathrm{CH_4,feed}} \left[y_{\mathrm{CH_4,raff}} \left(\Delta q_{\mathrm{CH_4}} + \Delta q_{\mathrm{CO_2}} \right) - \Delta q_{\mathrm{CH_4}} \right]} \right) \\ &= \frac{y_{\mathrm{CH_4,raff}} \left[y_{\mathrm{CH_4,feed}} \left(\Delta q_{\mathrm{CH_4}} + \Delta q_{\mathrm{CO_2}} \right) - \Delta q_{\mathrm{CH_4}} \right]}{y_{\mathrm{CH_4,feed}} \left[y_{\mathrm{CH_4,raff}} \left(\Delta q_{\mathrm{CH_4}} + \Delta q_{\mathrm{CO_2}} \right) - \Delta q_{\mathrm{CH_4}} \right]} \end{aligned} \tag{2}$$

Finally:

$$\begin{aligned} \frac{M_{\mathrm{ads}}}{M_{\mathrm{CH_4,raff}}} &= \frac{M_{\mathrm{ads}}}{M_{\mathrm{CH_4,feed}}} \div \frac{M_{\mathrm{CH_4,raff}}}{M_{\mathrm{CH_4,feed}}} \\ &= \frac{y_{\mathrm{CH_4,raff}} - y_{\mathrm{CH_4,feed}}}{y_{\mathrm{CH_4,raff}} \left[y_{\mathrm{CH_4,feed}} \left(\Delta q_{\mathrm{CH_4}} + \Delta q_{\mathrm{CO_2}} \right) - \Delta q_{\mathrm{CH_4}} \right]} \end{aligned} \tag{3}$$

Since $\frac{M_{\mathrm{CH_4,raff}}}{M_{\mathrm{CH_4,feed}}}$ is included as part of $\frac{M_{\mathrm{ads}}}{M_{\mathrm{CH_4,raff}}}$, which in turn is included in the equation for SPP, one could reasonably exclude the fractional CH_4 recovery term from appearing directly in the equation for SPP. However, a high fractional CH_4 recovery is desirable for more than direct economic costs, as any CH_4 not captured will likely be emitted and can be considered to be an environmental cost. Thus, we choose to directly include the fractional CH_4 recovery term in our equation for SPP.

3 Supplementary Figures

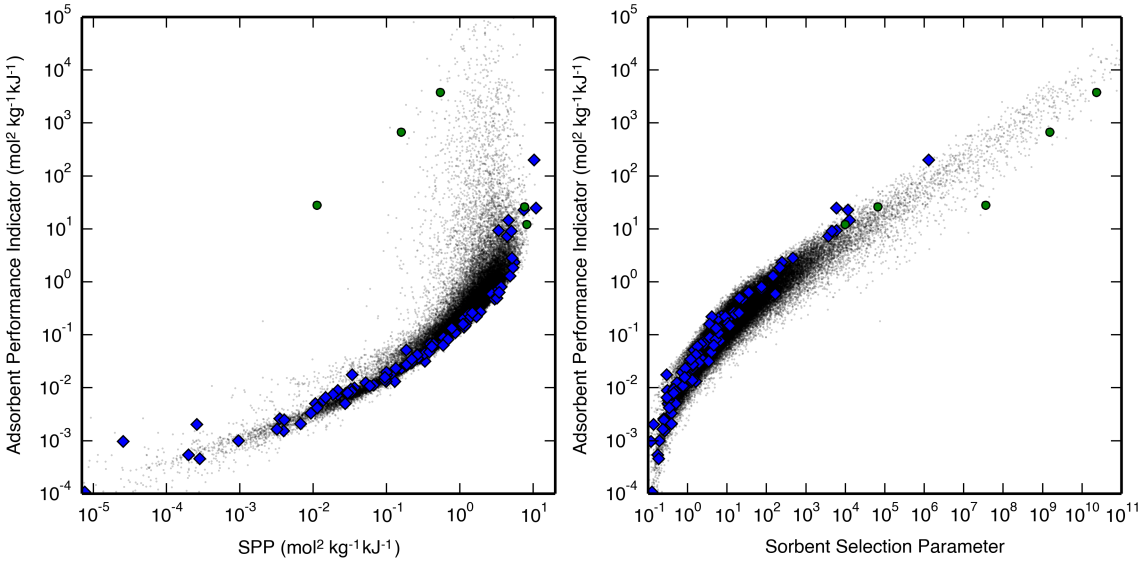

Fig. S1: (left) A correlation between the SPP and the Adsorbent Performance Indicator and (right) between the Sorbent Selection Parameter and the Adsorbent Performance Indicator, both for the APG process carried out with PSA. Hypothetical zeolites are shown as black dots, IZA zeolites are shown as blue diamonds, and the hypothetical zeolites shown in Table 1 are shown as green circles.

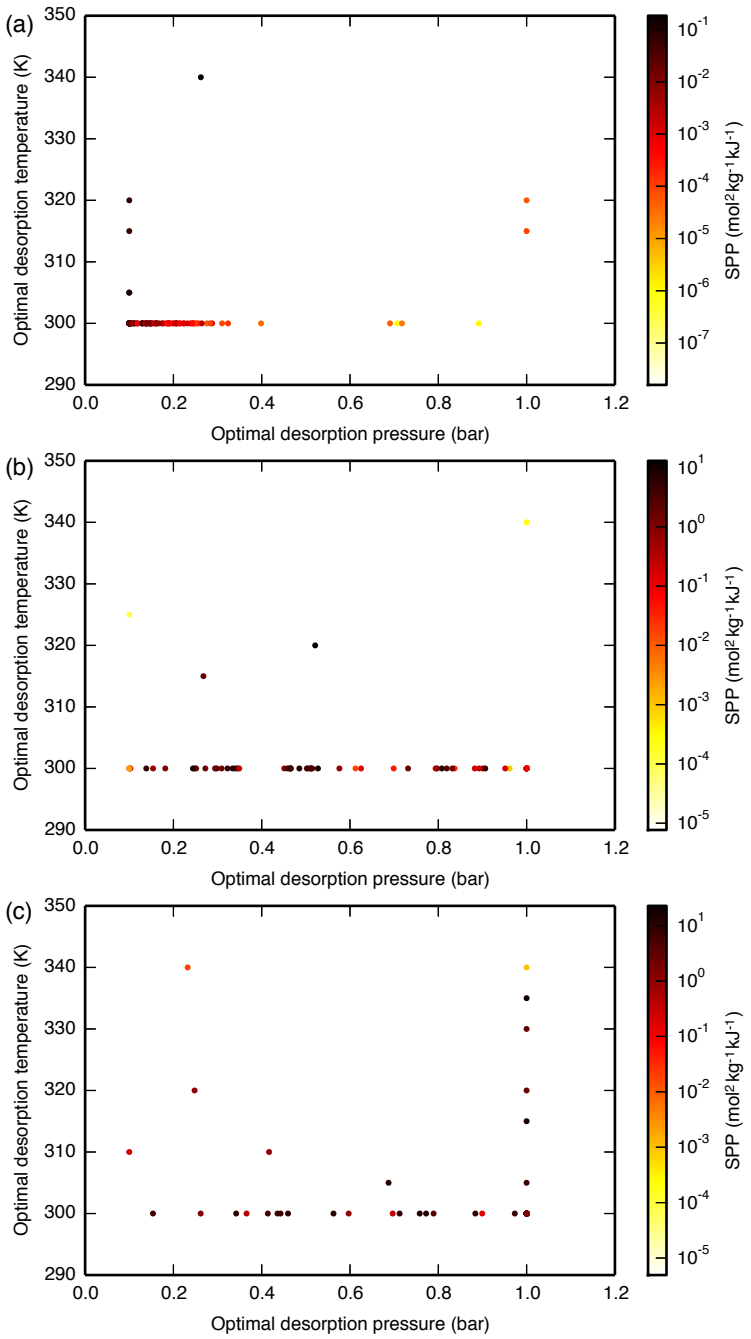

Fig. S2: SPP of the IZA zeolites for the (a) LFG, (b) APG, and (c) NAG processes carried out with PTSA as a function of the optimal desorption pressure and temperature. Note that the APG and NAG processes have several data points overlapping at 1 bar and 300 K. For the LFG process, a clear correlation exists between the desorption conditions and the SPP: zeolites with lower optimized desorption pressures are also better-performing. By comparing the SPP values of these materials at their optimal desorption conditions with the SPP values of these materials at set desorption conditions of 0.1 bar and 300 K (Fig. S30) it becomes clear that it was not the lowered desorption pressure that caused some materials to perform better than others; rather, top-performing materials have more to gain by pulling additional vacuum than do the poor-performing materials.

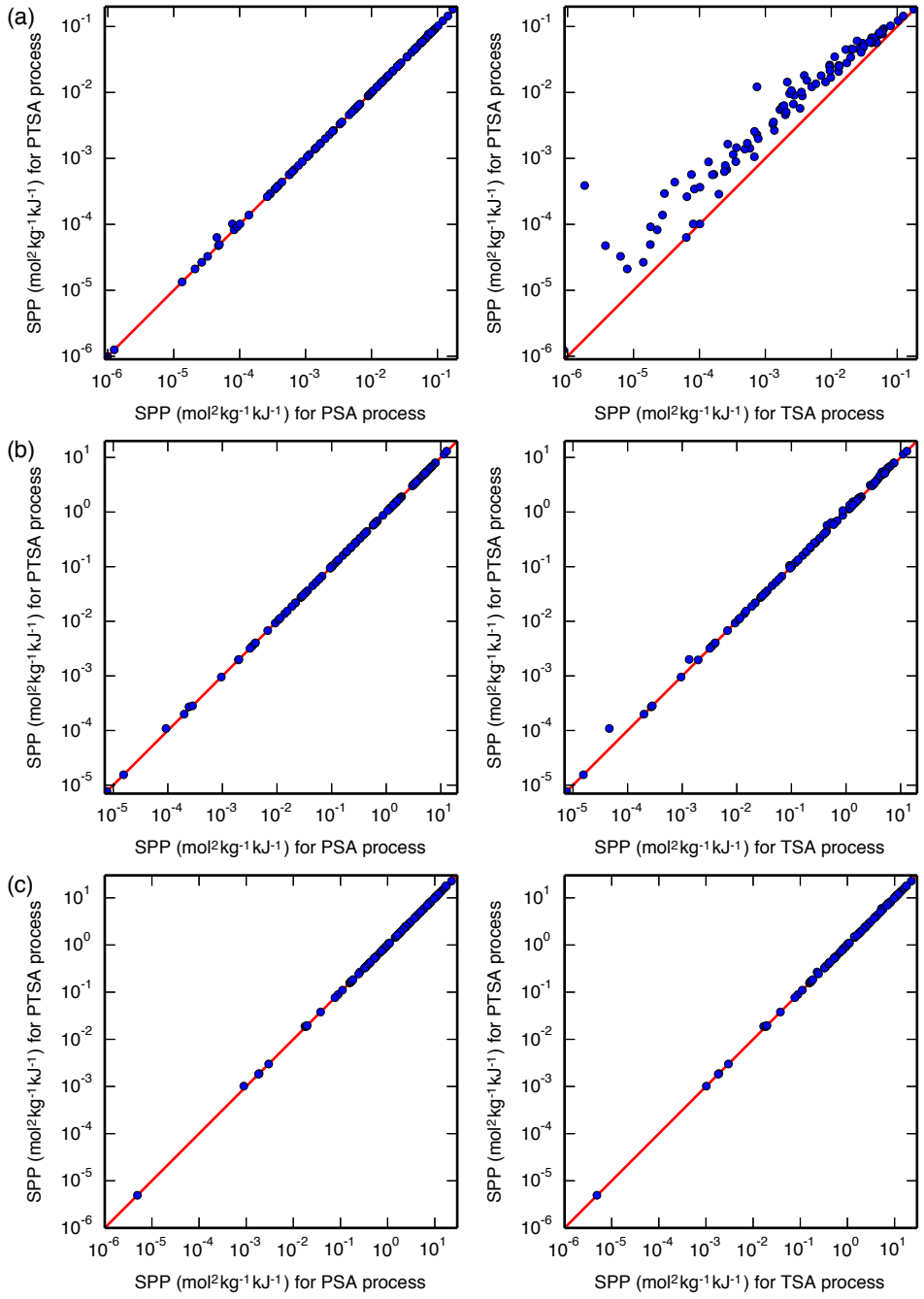

Fig. S3: SPP of the IZA zeolites for the (a) LFG, (b) APG, and (c) NAG processes carried out with PTSA at optimal desorption temperatures and pressures is plotted (left) against the SPP of the same process carried out with PSA at a set desorption temperature of 300 K and an optimal desorption pressure or (right) against the SPP of the same process carried out with TSA at an optimal desorption temperature and a set desorption pressure of 1 bar. Of the TSA processes, only the LFG process appears to have benefited from pulling vacuum, while the two higher-pressure processes received a "free" pressure-swing down to 1 bar, and thus do not benefit as much from the additional vacuum. A line is drawn at $y = x$ for reference.

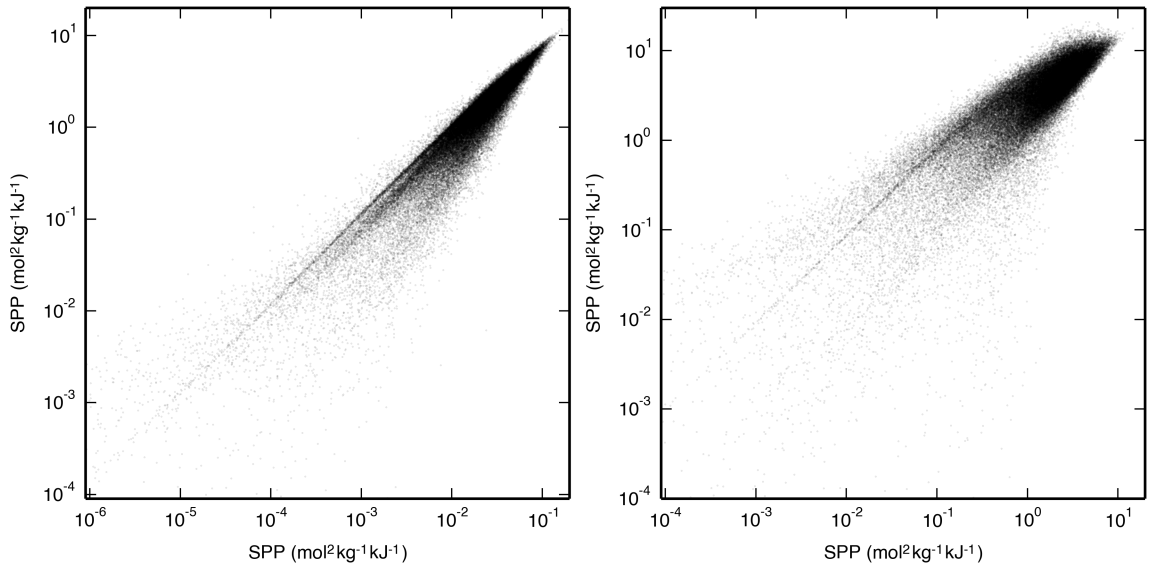

Fig. S4: SPP of the hypothetical zeolites for the (a) LFG and APG processes and for the (b) APG and NAG processes, all carried out with PSA.

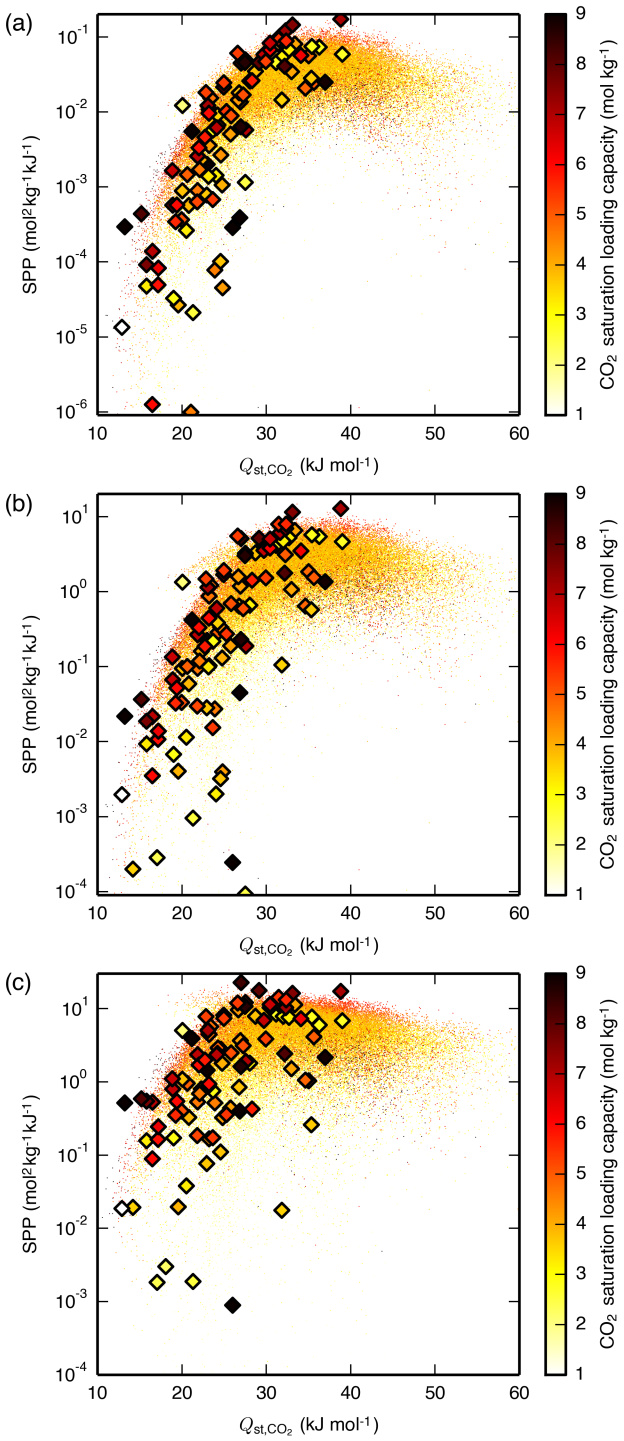

Fig. S5: SPP as a function of $Q_{\mathrm{st,CO_2}}$ and the CO_2 saturation loading capacity, for the (a) LFG, (b) APG, and (c) NAG processes, all carried out with PSA. The materials are plotted in random order such that the data shown are representative of the materials hidden due to having similar $Q_{\mathrm{st,CO_2}}$ and SPP. IZA zeolites are shown as diamonds. This plot is the same as in Fig. 2, but with the IZA zeolites overlaid.

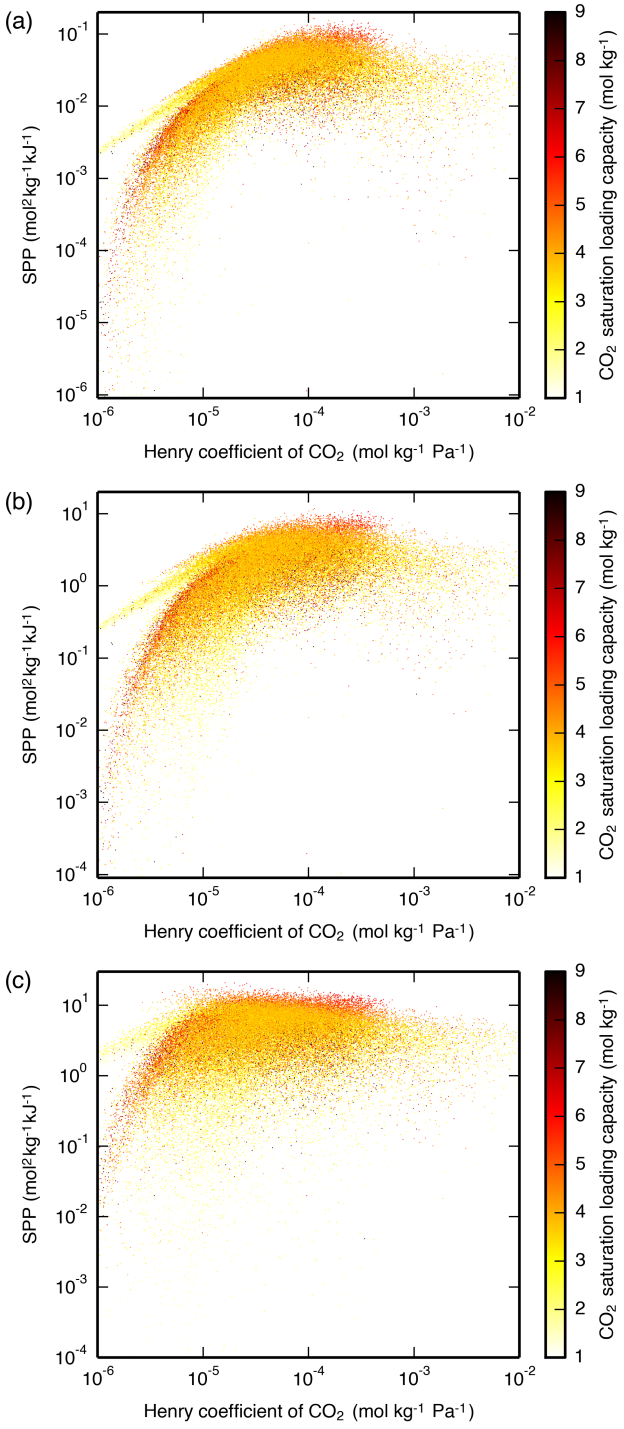

Fig. S6: SPP of the hypothetical zeolites as a function of the Henry coefficient and CO_2 saturation loading capacity, for the (a) LFG, (b) APG, and (c) NAG processes, all carried out with PSA. The materials are plotted in random order such that the data shown are representative of the materials hidden due to having similar $Q_{\mathrm{st,CO_2}}$ and SPP.

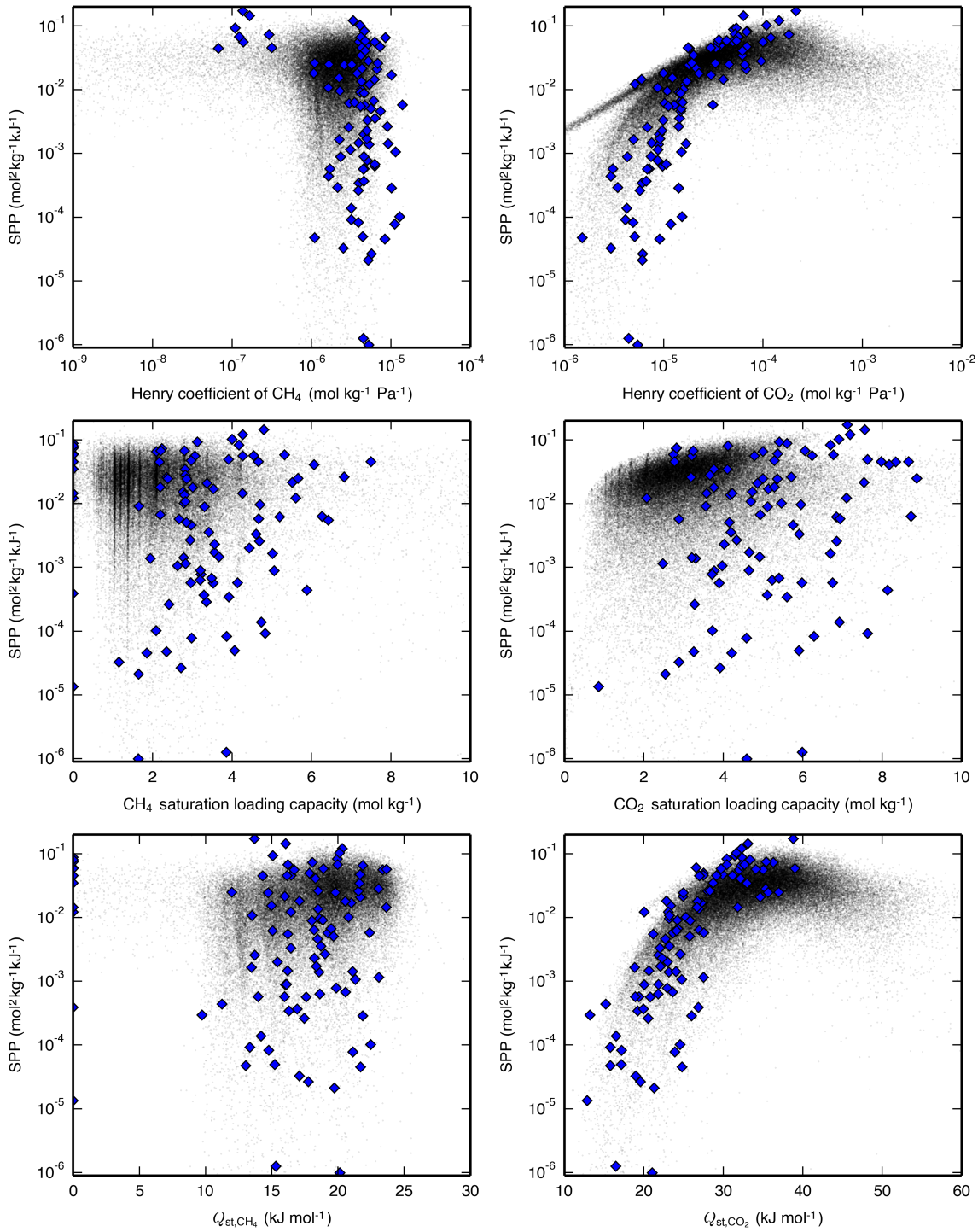

Fig. S7: SPP as a function of Henry coefficients, saturation loadings, and Q_{st} for the LFG process carried out with PSA. Hypothetical zeolites are shown as black dots, and IZA zeolites are shown as blue diamonds. The stripes seen in plots containing CH_4 saturation loading capacity are due to that variable being more likely to be integer values of CH_4 molecules per unit cell (Fig. S10).

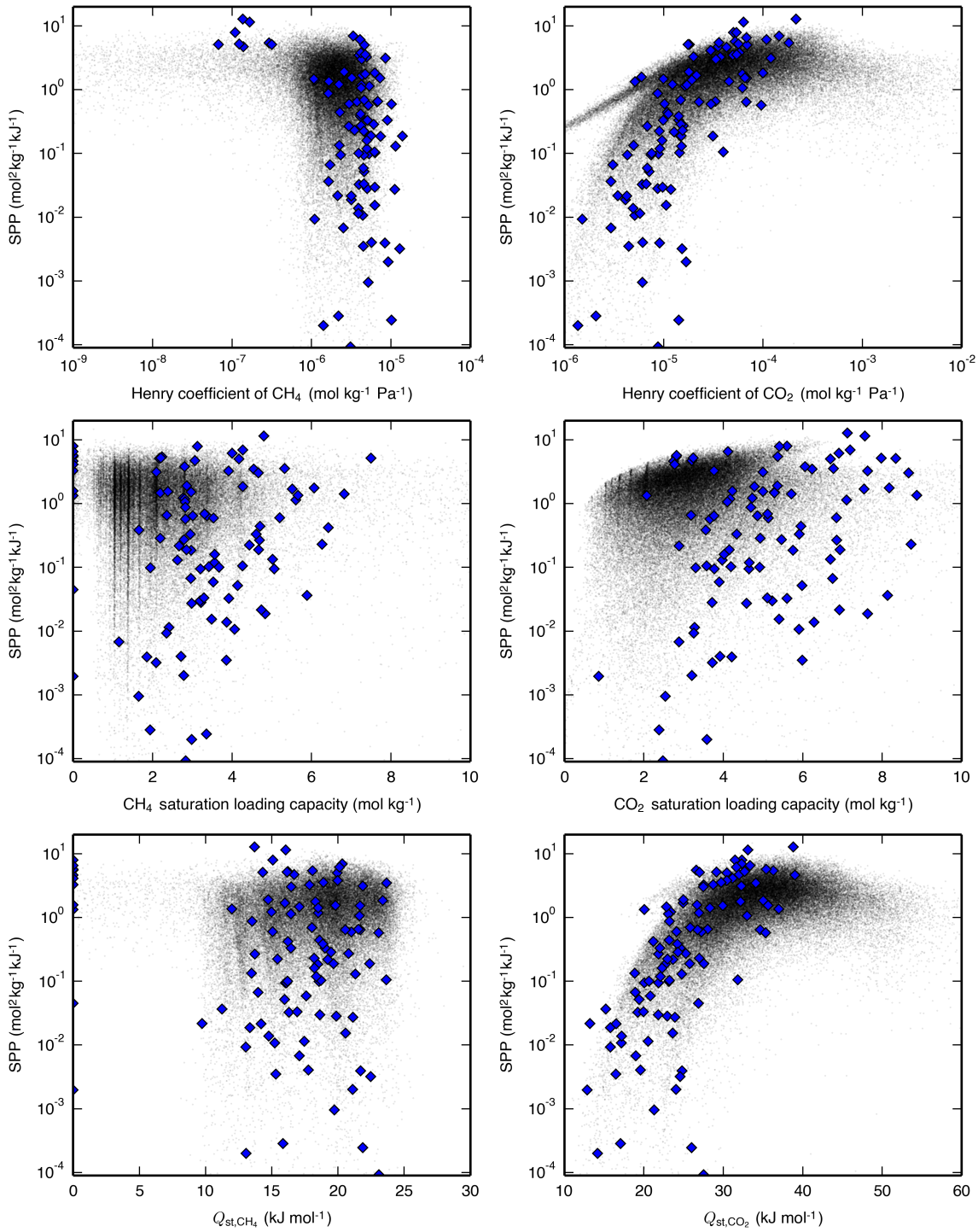

Fig. S8: SPP as a function of Henry coefficients, saturation loadings, and Q_{st} for the APG process carried out with PSA. Hypothetical zeolites are shown as black dots, and IZA zeolites are shown as blue diamonds. The stripes seen in plots containing CH_4 saturation loading capacity are due to that variable being more likely to be integer values of CH_4 molecules per unit cell (Fig. S10).

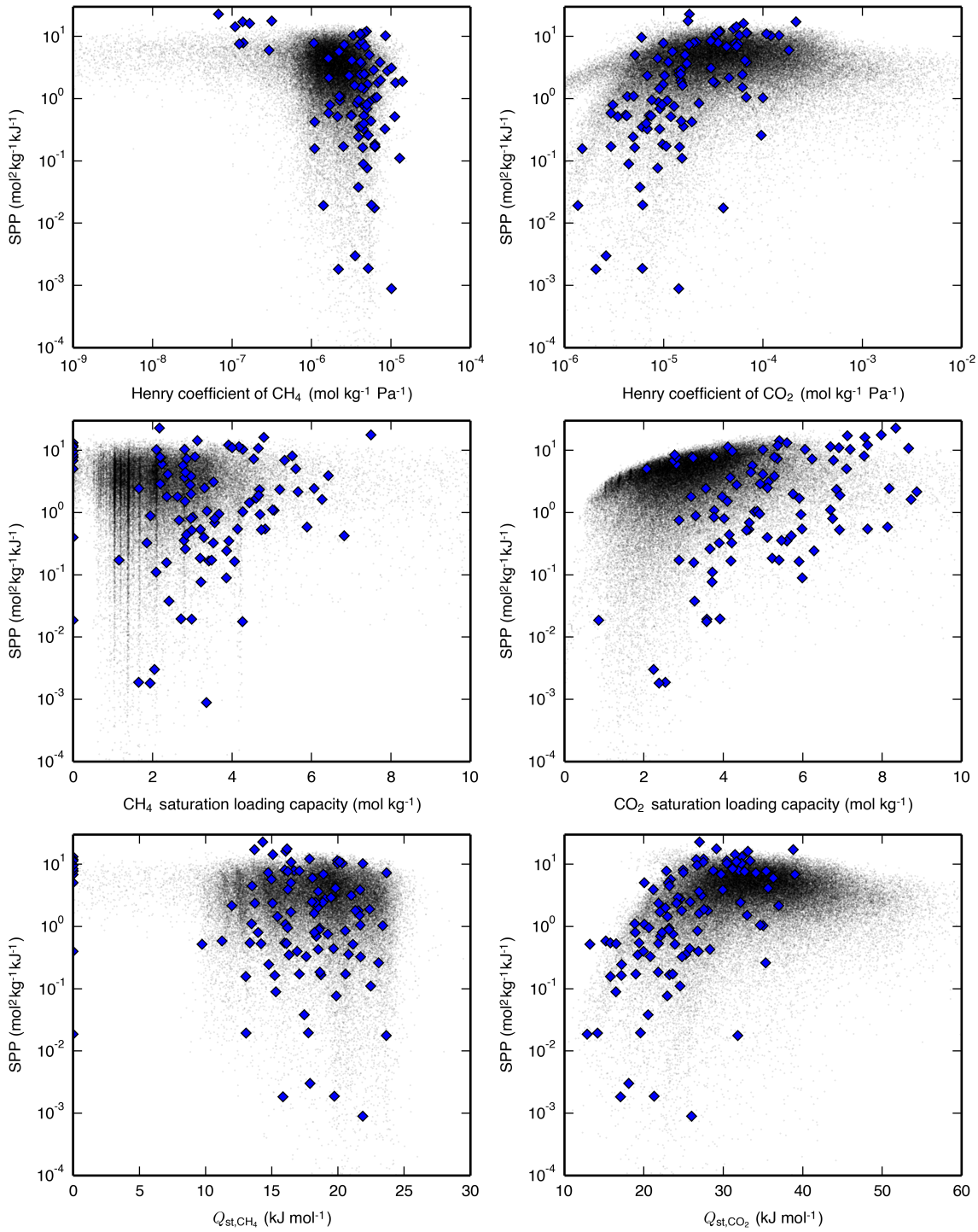

Fig. S9: SPP as a function of Henry coefficients, saturation loadings, and Q_{st} for the NAG process carried out with PSA. Hypothetical zeolites are shown as black dots, and IZA zeolites are shown as blue diamonds. The stripes seen in plots containing CH_4 saturation loading capacity are due to that variable being more likely to be integer values of CH_4 molecules per unit cell (Fig. S10).

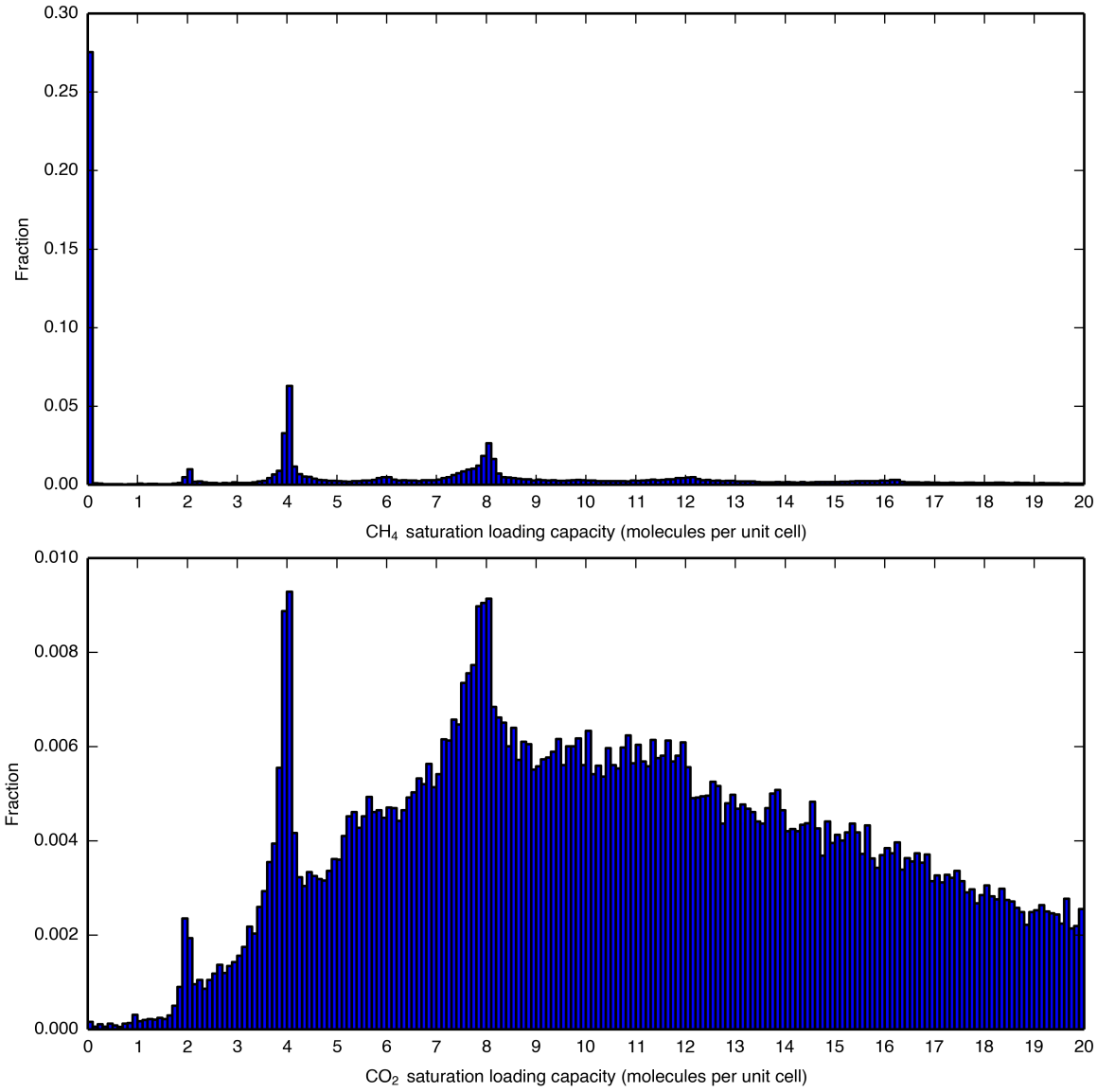

Fig. S10: The distribution of (top) CH_4 saturation loading capacities for the hypothetical zeolites shows that even integer values in units of molecules per unit cell are most common, a trend which is less noticeable for (bottom) CO_2 saturation loading capacities. This explains the stripes seen in Figs. 5, S7–S9, and S13 in the plots containing CH_4 saturation loading capacity. Both histograms have been truncated at 20 molecules per unit cell.

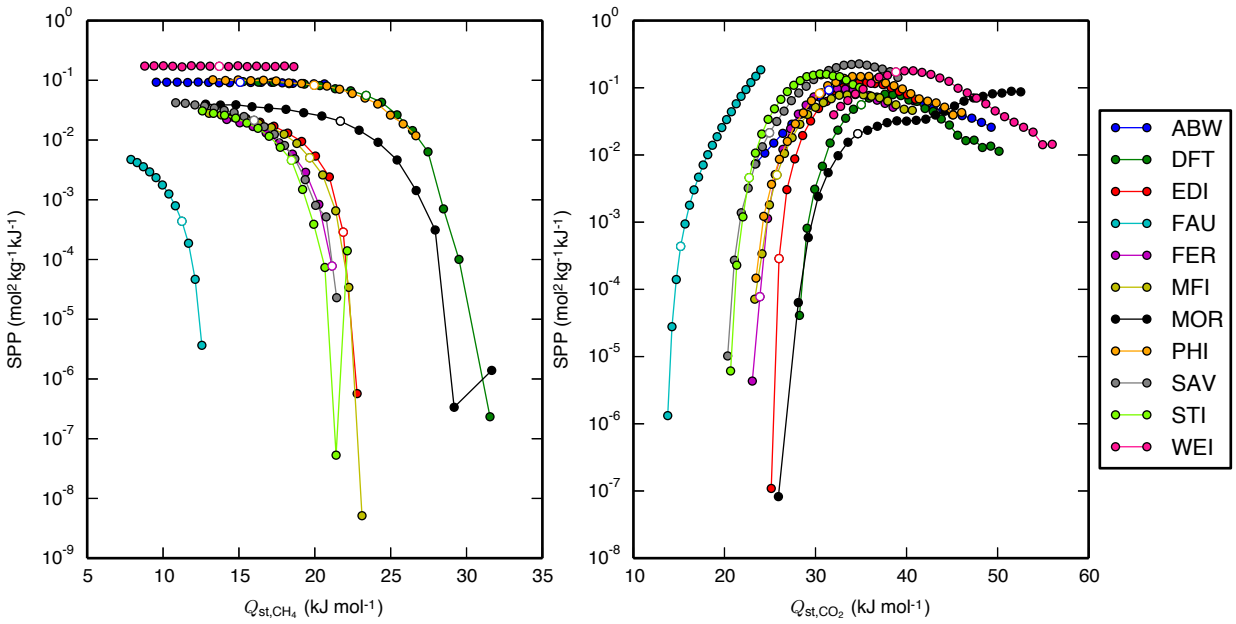

Fig. S11: SPP of a subset of IZA zeolites undergoing the LFG PSA process as a function of (left) $Q_{\mathrm{st,CH_4}}$ and (right) $Q_{\mathrm{st,CO_2}}$. The points with white marker color represent the data with original guest-host epsilon parameters of the Lennard-Jones potential (115.00 K for CH_4-O_{zeo}, 50.20 K for C_{CO_2}-O_{zeo}, and 84.93 K for O_{CO_2}-O_{zeo}). (left) The CH_4-O_{zeo} epsilon value was varied between 75 K and 155 K in increments of 5 K (4.35 % of the original value), with larger values resulting in a larger $Q_{\mathrm{st,CH_4}}$. (right) The C_{CO_2}-O_{zeo} epsilon value was varied between 32.128 K and 88.603 K in increments of 2.259 K while the O_{CO_2}-O_{zeo} epsilon value was concurrently varied between 54.354 K and 149.904 K in increments of 3.822 K (both 4.50 % of the original values), with larger values resulting in a larger $Q_{\mathrm{st,CO_2}}$. When $Q_{\mathrm{st,CH_4}}$ was brought too high or $Q_{\mathrm{st,CO_2}}$ was brought too low, the material would become unfit for the separation, so these points are not shown. Note that SPP of the zeolite WEI does not change with $Q_{\mathrm{st,CH_4}}$ because CH_4 loading is negligibly low at all $Q_{\mathrm{st,CH_4}}$ values.

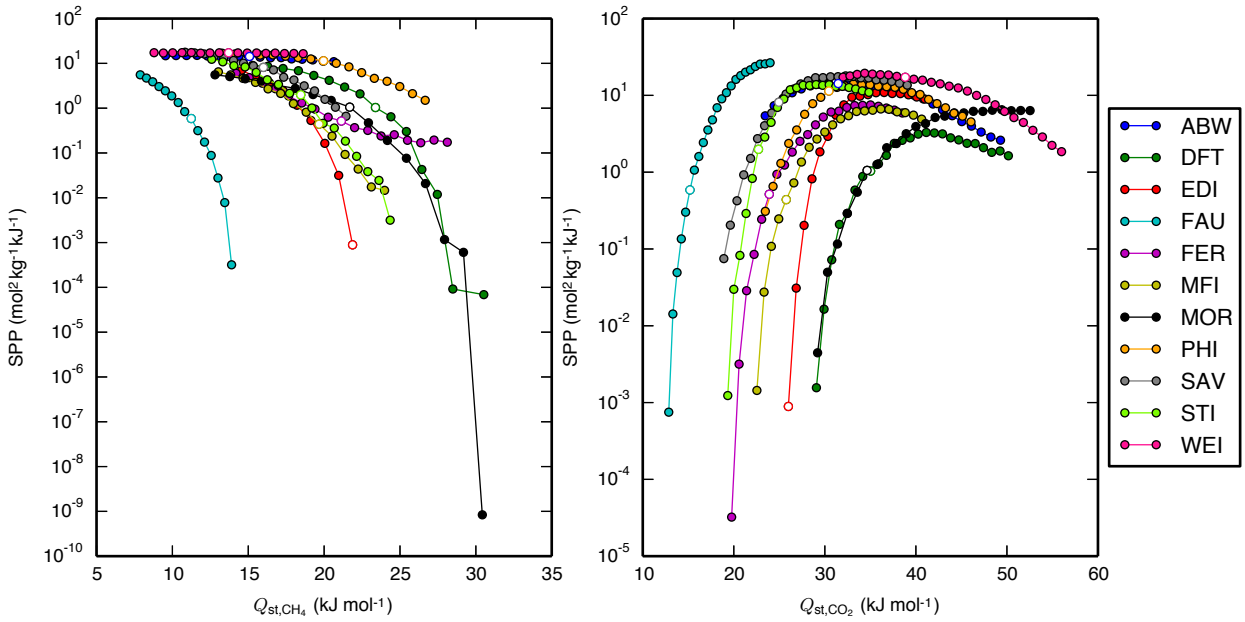

Fig. S12: SPP of a subset of IZA zeolites undergoing the NAG PSA process as a function of (left) $Q_{\mathrm{st,CH_4}}$ and (right) $Q_{\mathrm{st,CO_2}}$. The points with white marker color represent the data with original guest-host epsilon parameters of the Lennard-Jones potential (115.00 K for CH_4-O_{zeo}, 50.20 K for C_{CO_2}-O_{zeo}, and 84.93 K for O_{CO_2}-O_{zeo}). (left) The CH_4-O_{zeo} epsilon value was varied between 75 K and 155 K in increments of 5 K (4.35 % of the original value), with larger values resulting in a larger $Q_{\mathrm{st,CH_4}}$. (right) The C_{CO_2}-O_{zeo} epsilon value was varied between 32.128 K and 88.603 K in increments of 2.259 K while the O_{CO_2}-O_{zeo} epsilon value was concurrently varied between 54.354 K and 149.904 K in increments of 3.822 K (both 4.50 % of the original values), with larger values resulting in a larger $Q_{\mathrm{st,CO_2}}$. When $Q_{\mathrm{st,CH_4}}$ was brought too high or $Q_{\mathrm{st,CO_2}}$ was brought too low, the material would become unfit for the separation, so these points are not shown. Note that SPP of the zeolite WEI does not change with $Q_{\mathrm{st,CH_4}}$ because CH_4 loading is negligibly low at all $Q_{\mathrm{st,CH_4}}$ values.

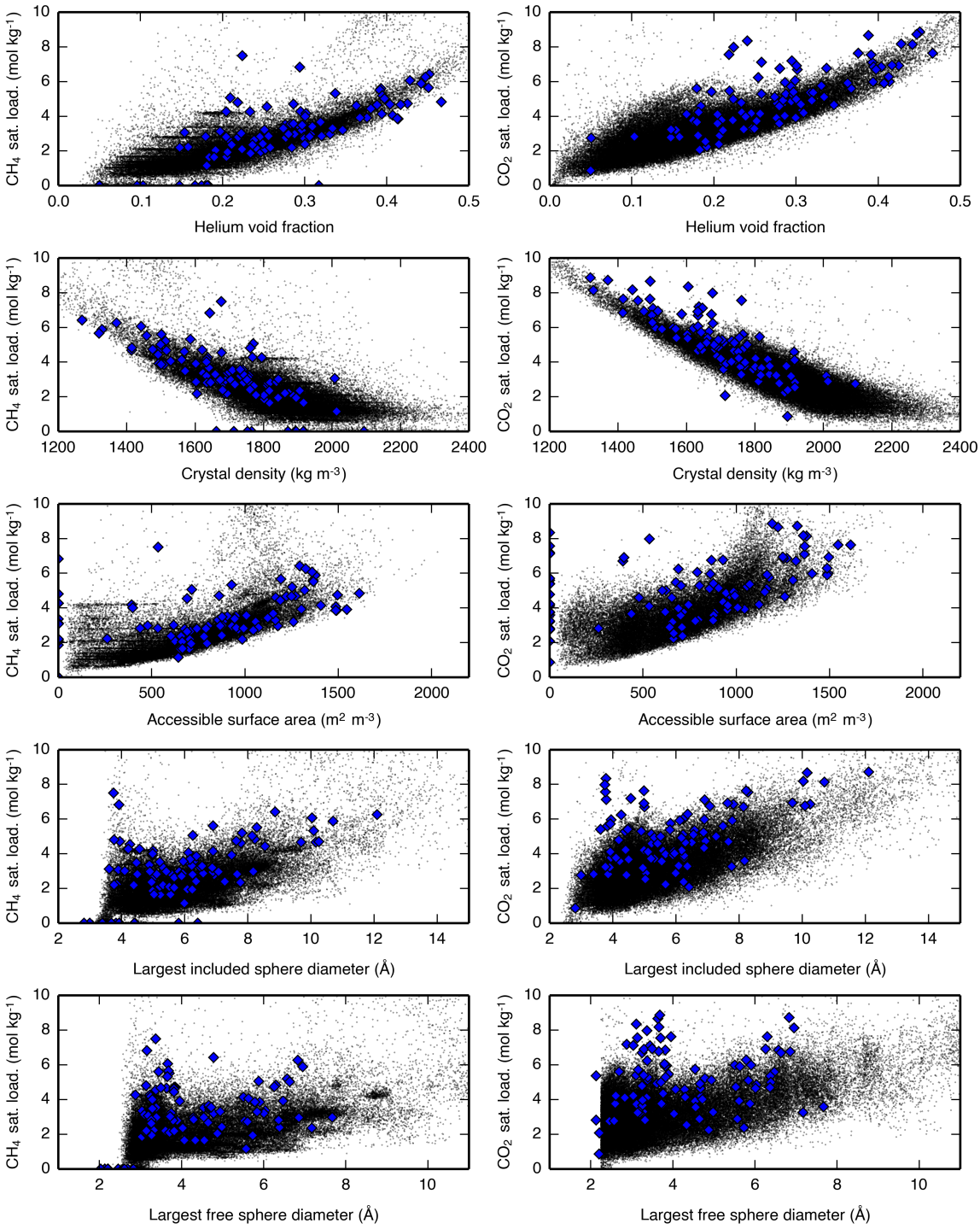

Fig. S13: Relationships between a zeolite's geometric descriptors and its saturation loading capacities. Hypothetical zeolites are shown as black dots, and IZA zeolites are shown as blue diamonds. The stripes seen in plots containing CH_4 saturation loading capacity are due to that variable being more likely to be integer values of CH_4 molecules per unit cell (Fig. S10).

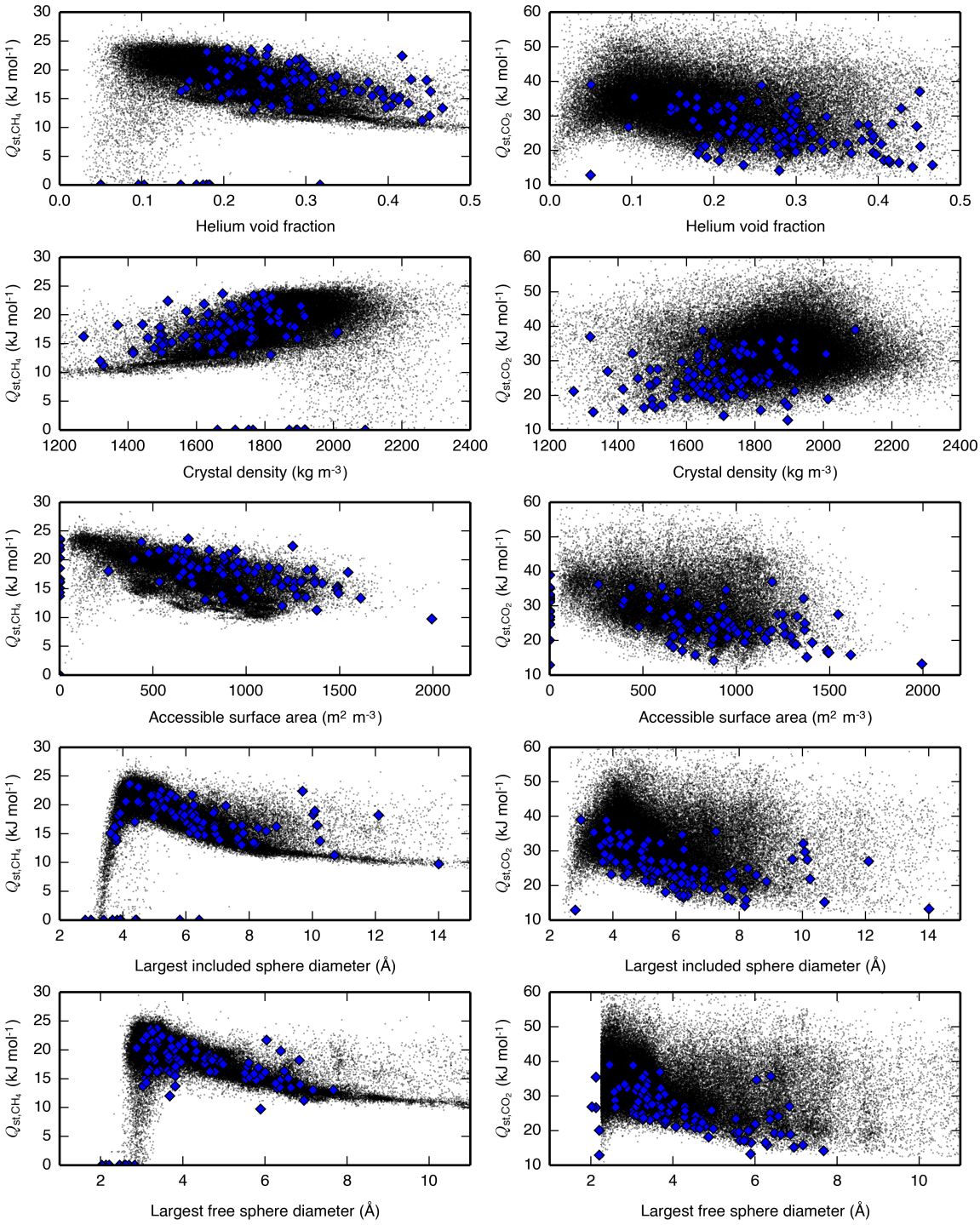

Fig. S14: Relationships between a zeolite's geometric descriptors and Q_{st}. Hypothetical zeolites are shown as black dots, and IZA zeolites are shown as blue diamonds.

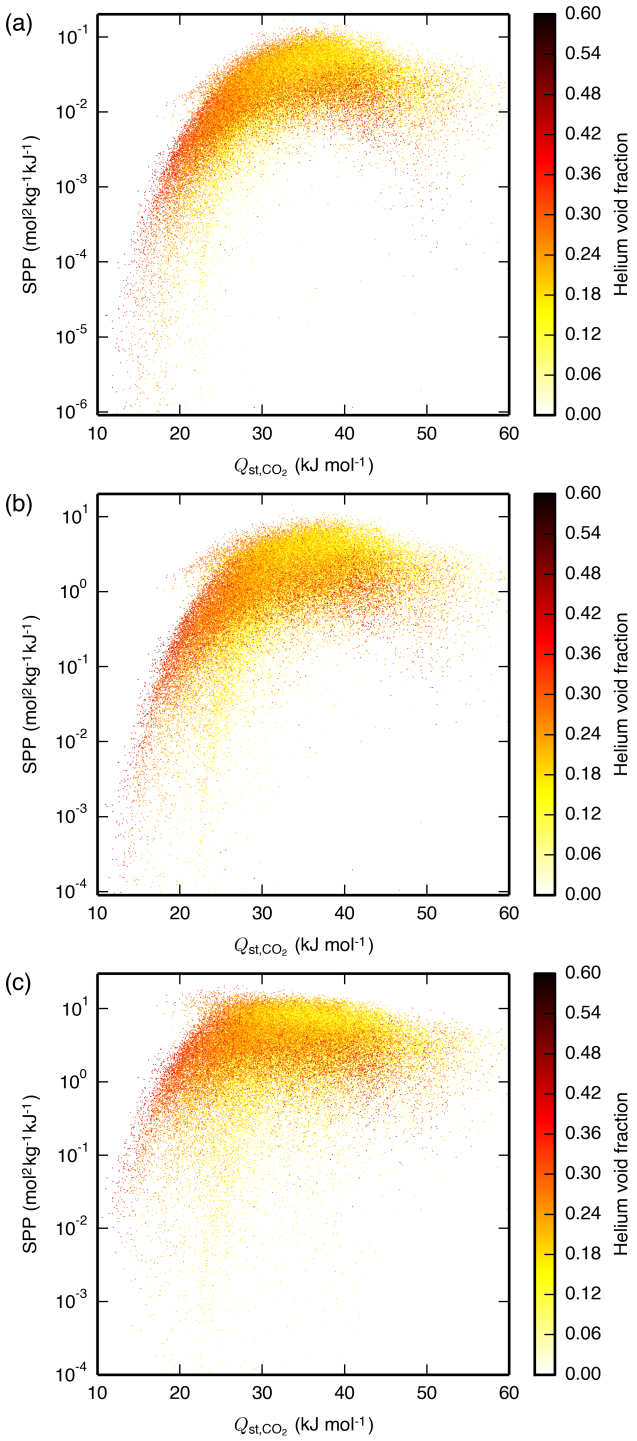

Fig. S15: SPP of the hypothetical zeolites as a function of $Q_{\mathrm{st,CO_2}}$ and helium void fraction, for the (a) LFG, (b) APG, and (c) NAG processes, all carried out with PSA. The materials are plotted in random order such that the data shown are representative of the materials hidden due to having similar $Q_{\mathrm{st,CO_2}}$ and SPP.

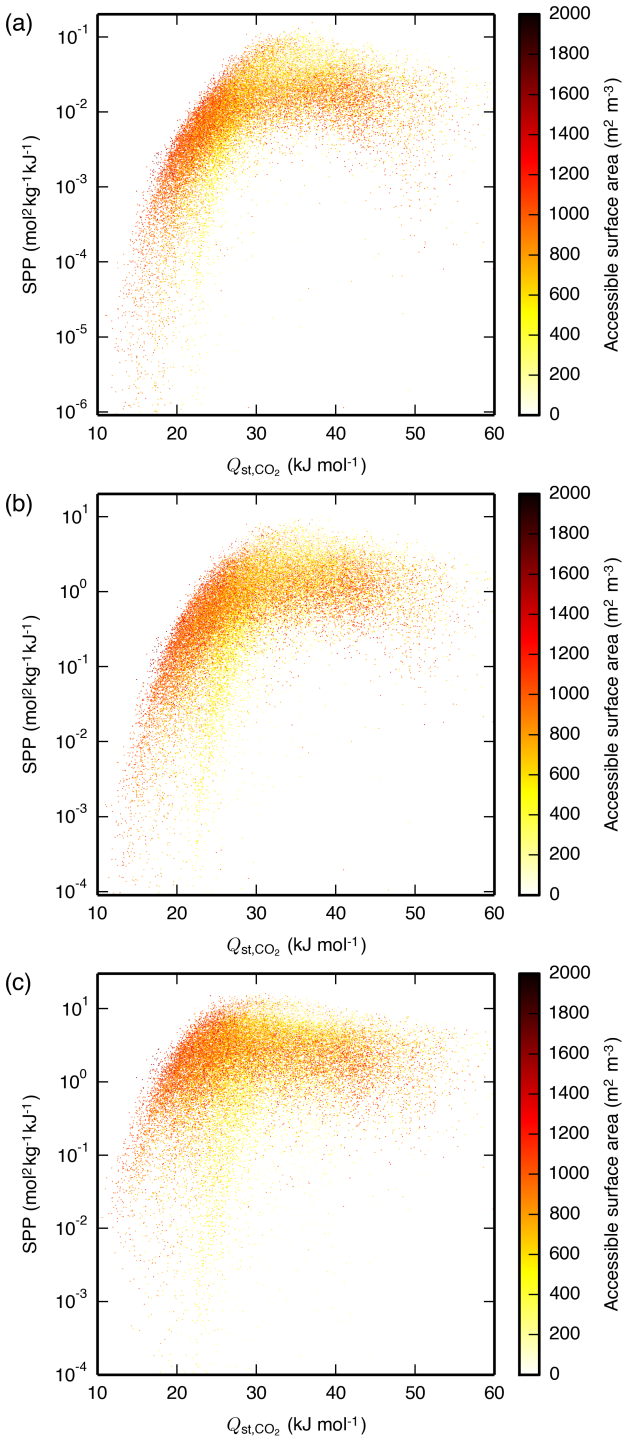

Fig. S16: SPP of the hypothetical zeolites as a function of $Q_{\mathrm{st,CO_2}}$ and accessible surface area, for the (a) LFG, (b) APG, and (c) NAG processes, all carried out with PSA. The materials are plotted in random order such that the data shown are representative of the materials hidden due to having similar $Q_{\mathrm{st,CO_2}}$ and SPP.

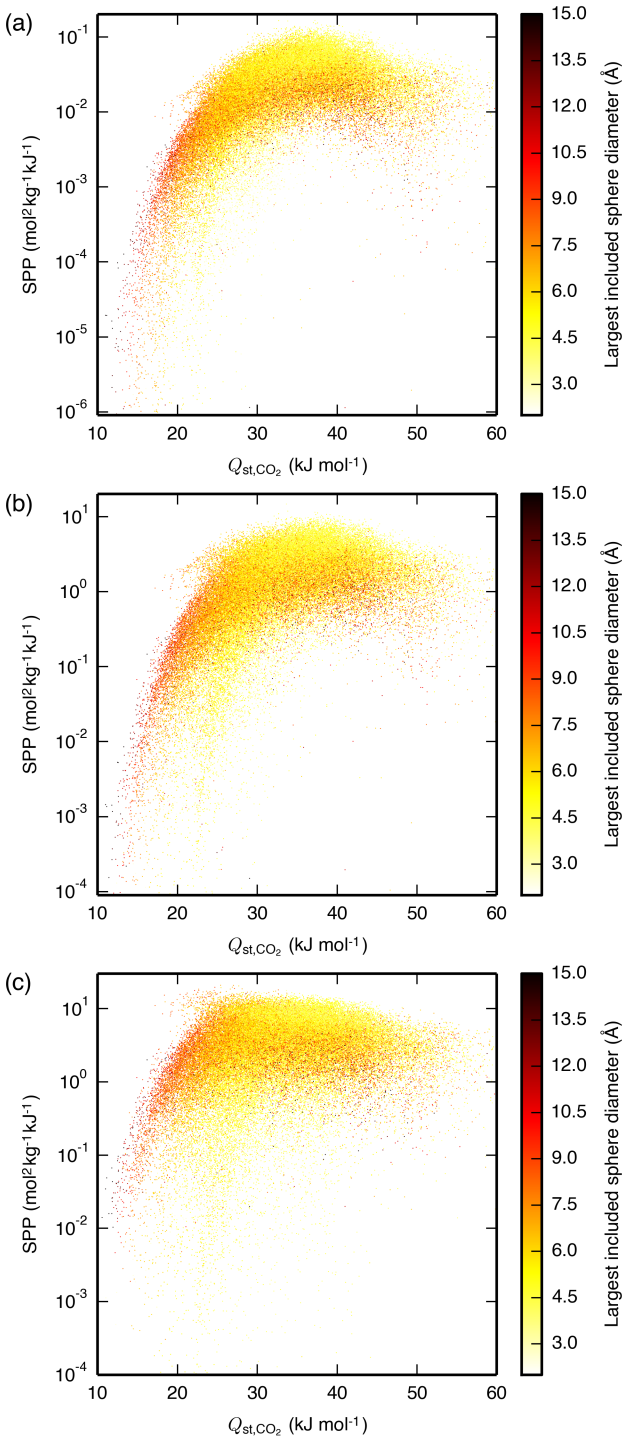

Fig. S17: SPP of the hypothetical zeolites as a function of Q_{st,CO_2} and largest included sphere diameter, for the (a) LFG, (b) APG, and (c) NAG processes, all carried out with PSA. The materials are plotted in random order such that the data shown are representative of the materials hidden due to having similar Q_{st,CO_2} and SPP.

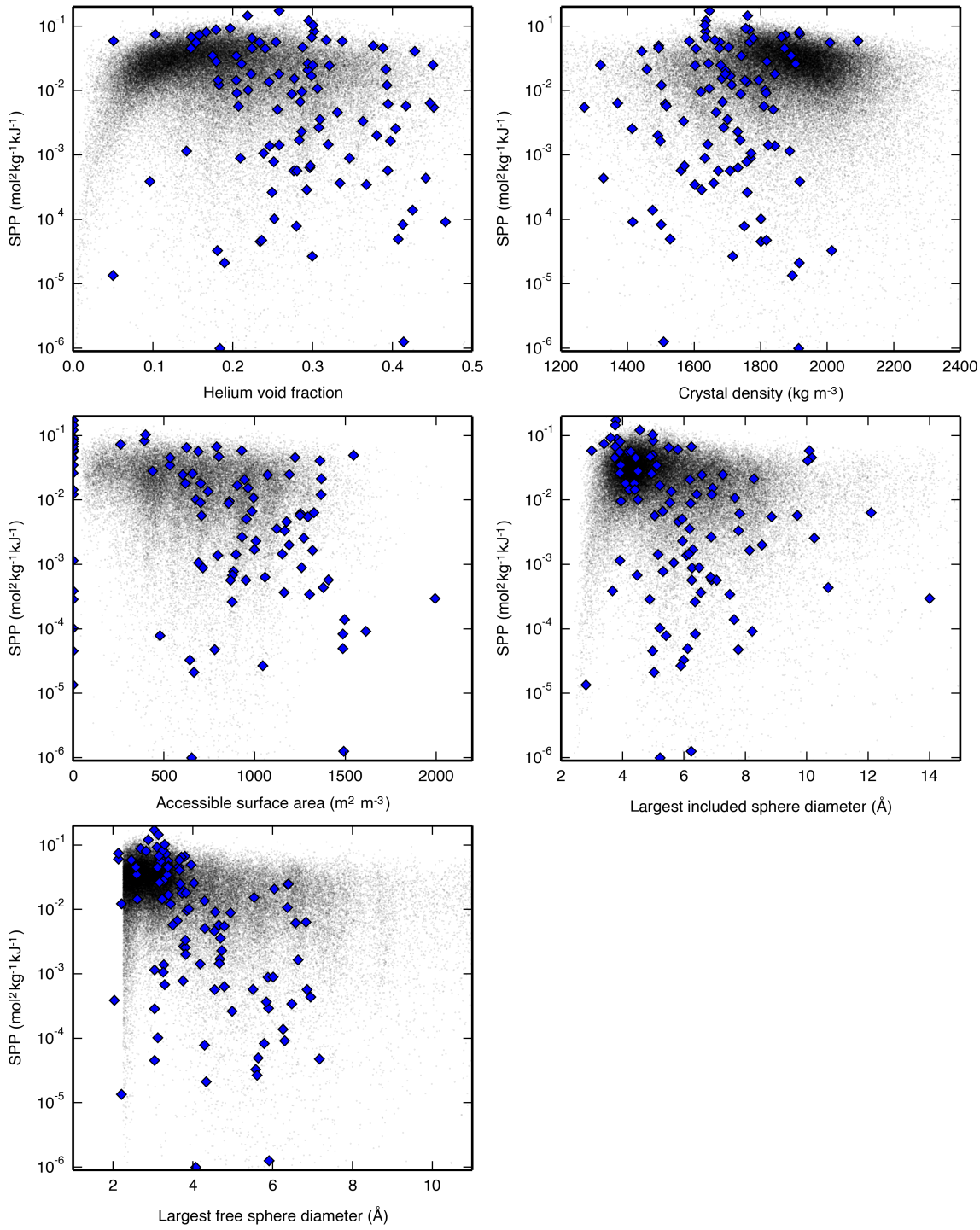

Fig. S18: SPP as a function of geometric parameters for the LFG process carried out with PSA. Hypothetical zeolites are shown as black dots, and IZA zeolites are shown as blue diamonds.

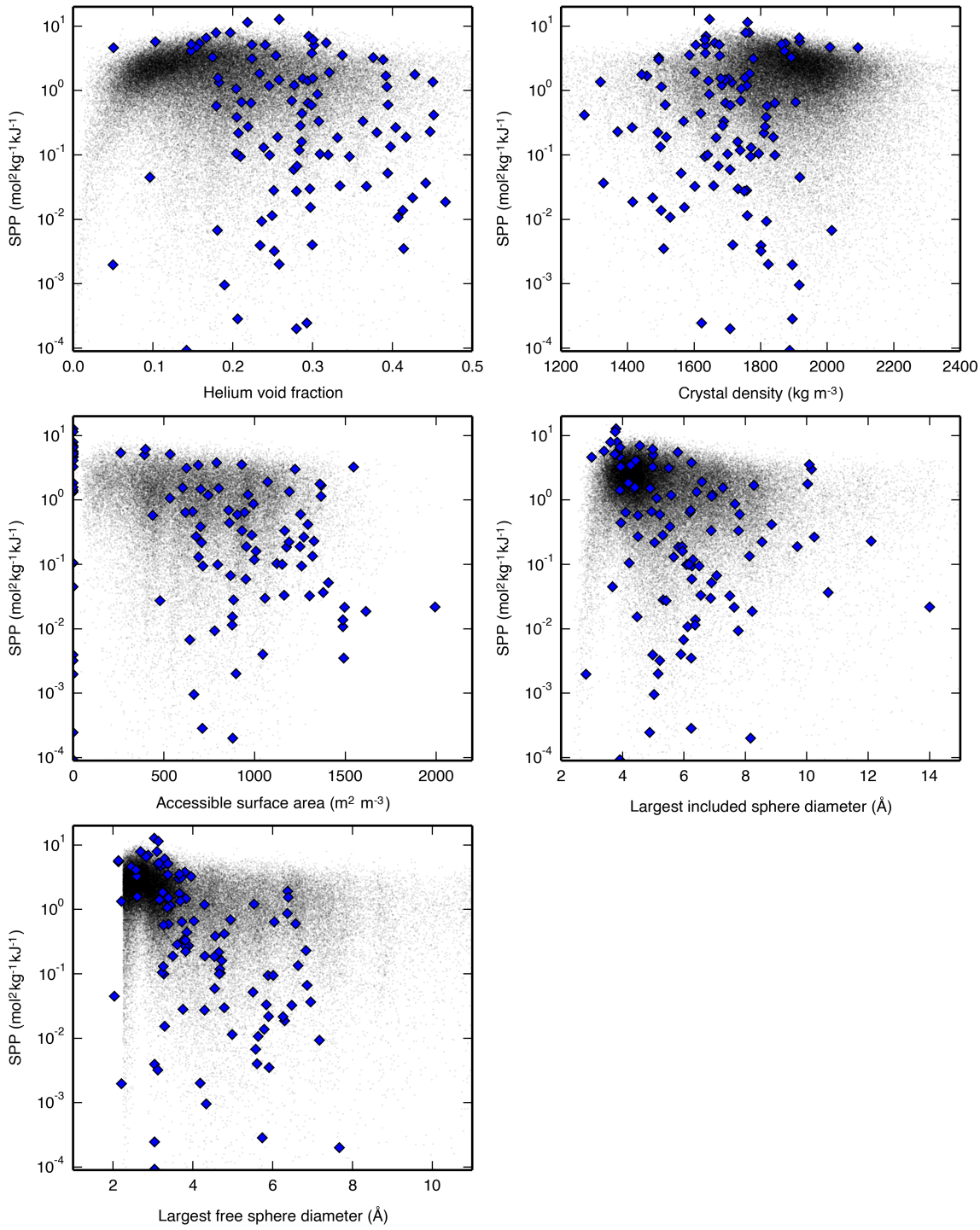

Fig. S19: SPP as a function of geometric parameters for the APG process carried out with PSA. Hypothetical zeolites are shown as black dots, and IZA zeolites are shown as blue diamonds.

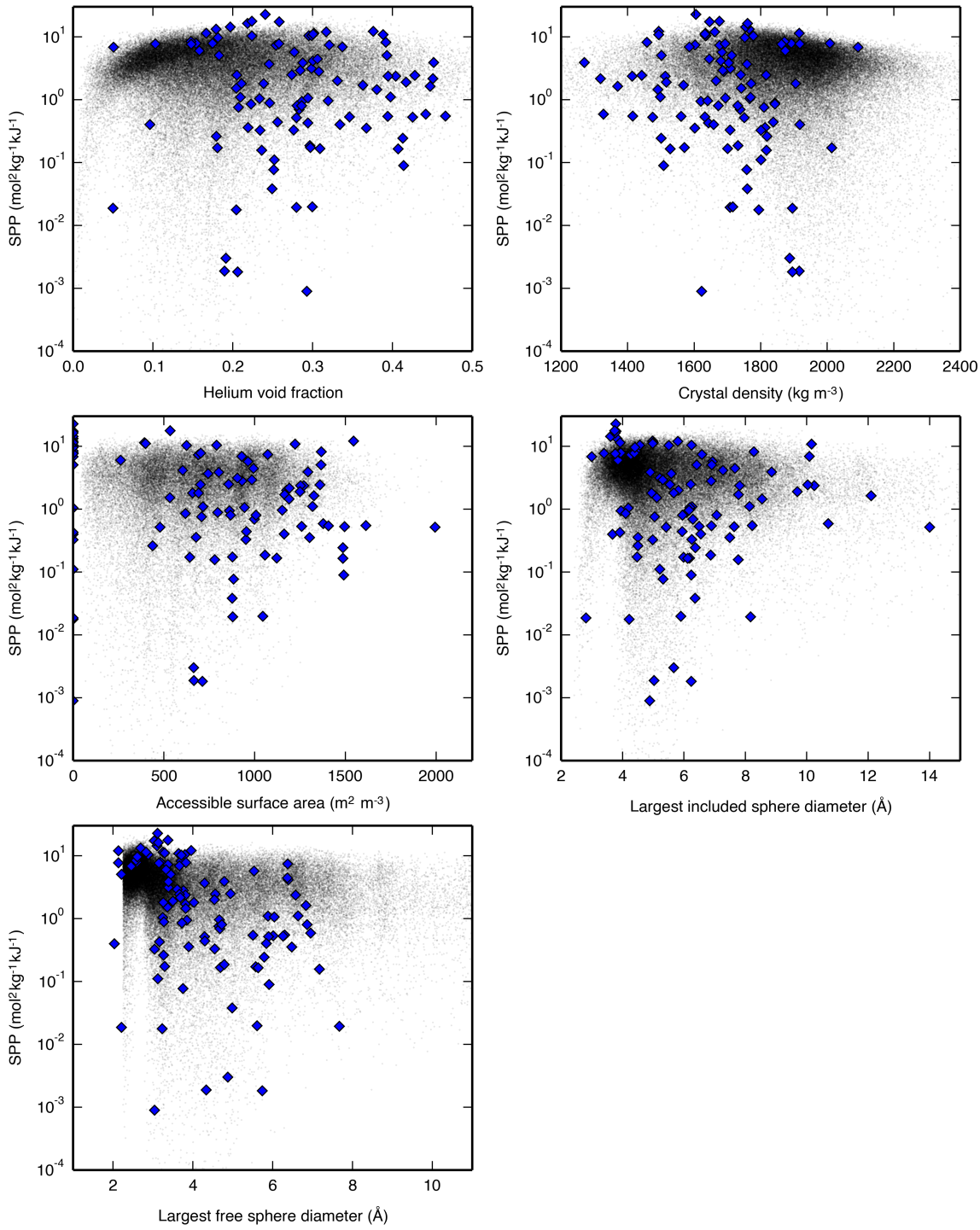

Fig. S20: SPP as a function of geometric parameters for the NAG process carried out with PSA. Hypothetical zeolites are shown as black dots, and IZA zeolites are shown as blue diamonds.

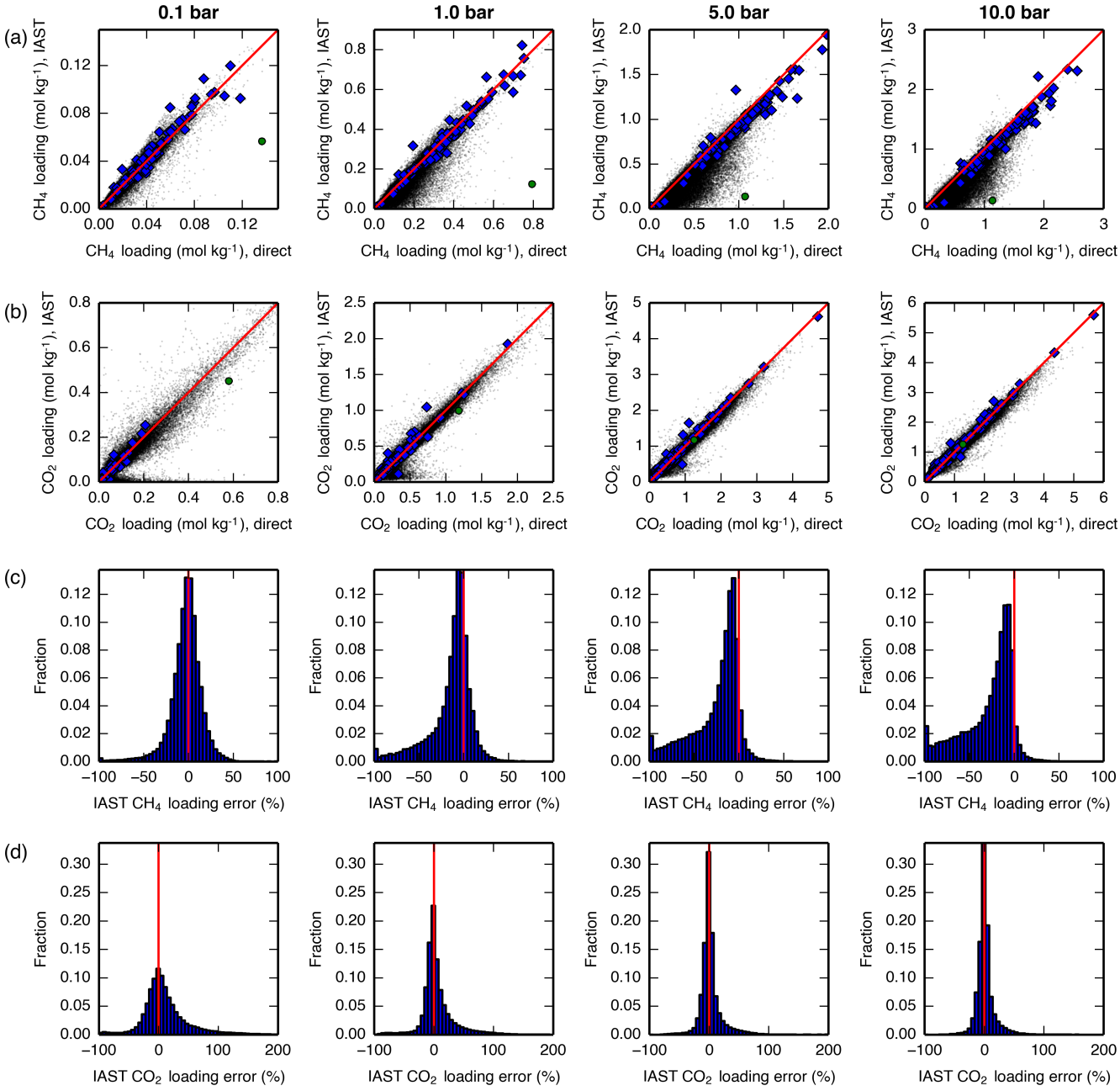

Fig. S21: Loadings of (a) CH_4 and (b) CO_2 at various total pressures, 300 K, and 90 mol % CH_4. Data on the x-axis are taken from directly-simulated mixture isotherms, while data on the y-axis are taken from applying IAST to pure-component isotherms. A line is drawn at $y = x$ for reference. Hypothetical zeolites are shown as black dots, IZA zeolites are shown as blue diamonds, and hypothetical zeolite PCOD8205017 is shown as a green circle. Histograms of the fractional IAST error $\left(\frac{\text{IAST loading} - \text{direct loading}}{\text{direct loading}} \times 100\%\right)$ of the hypothetical zeolites only for (c) CH_4 and (d) CO_2 at the same conditions. A line is drawn at $x = 0$ for reference. All plots in the left-column are at 0.1 bar, all plots in the middle-left-column are at 1 bar, all plots in the middle-right-column are at 5 bar, and all plots in the right-column are at 10 bar. A similar plot showing results at 60 mol % CH_4 is given in Fig. 7.

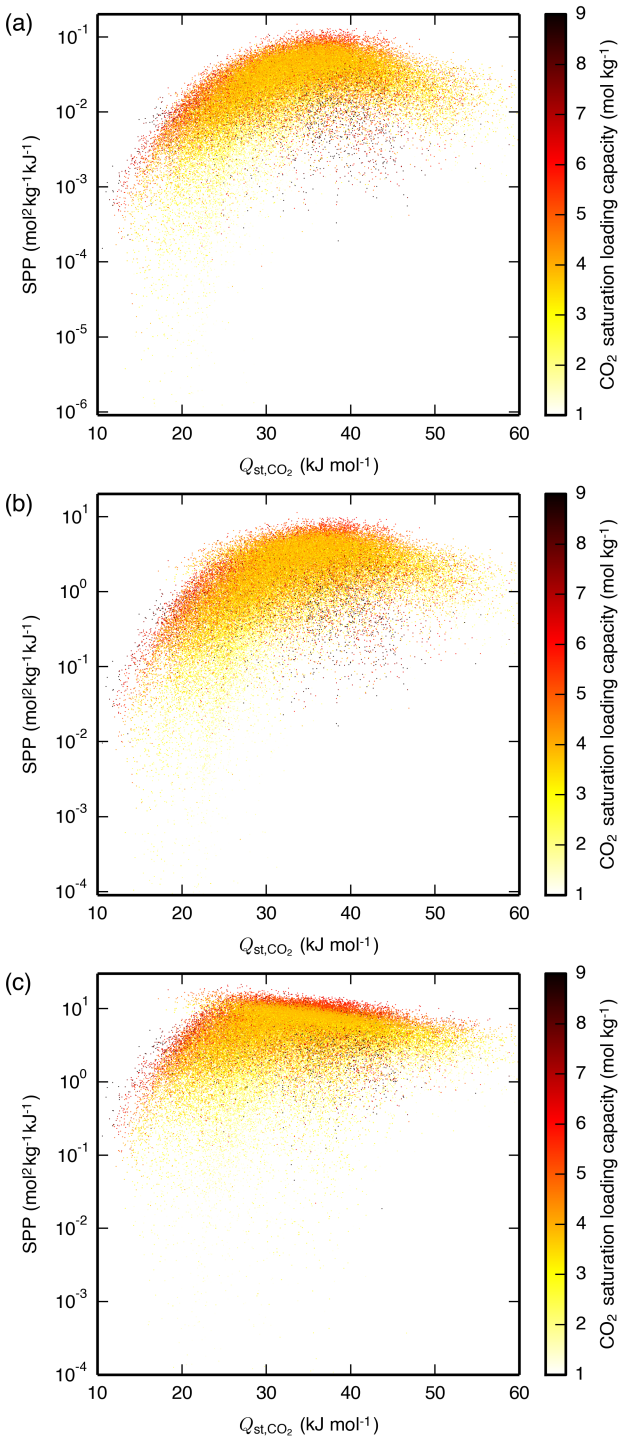

Fig. S22: SPP of the hypothetical zeolites as a function of $Q_{\mathrm{st,CO_2}}$ and the CO_2 saturation loading capacity for the (a) LFG, (b) APG, and (c) NAG processes, all carried out with PSA. The materials are plotted in random order such that the data shown are representative of the materials hidden due to having similar $Q_{\mathrm{st,CO_2}}$ and SPP. Mixture isotherms were obtained using IAST, whereas Fig. 2 used directly-generated mixture isotherms.

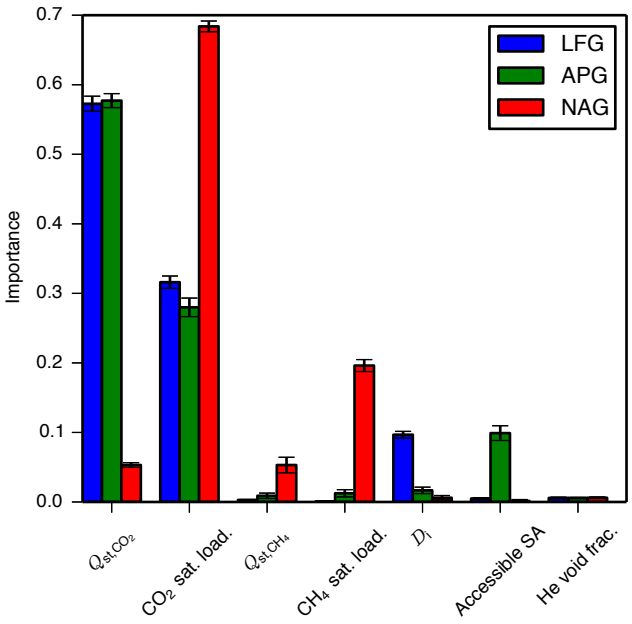

Fig. S23: Importance of geometric and isotherm descriptors to the SPP of the hypothetical zeolites undergoing PSA processes, as determined using a random forest of decision trees. The importance of a descriptor is calculated by summing the reductions in mean squared error brought about at each node where that descriptor splits a decision tree, averaging over all decision trees, and normalizing.[19] Here, sat. load. is the saturation loading capacity, D_i is the largest included sphere diameter, Accessible SA is the accessible surface area, and He void frac. is the helium void fraction. Mixture isotherms were obtained using IAST, whereas Fig. 4 used directly-generated mixture isotherms.

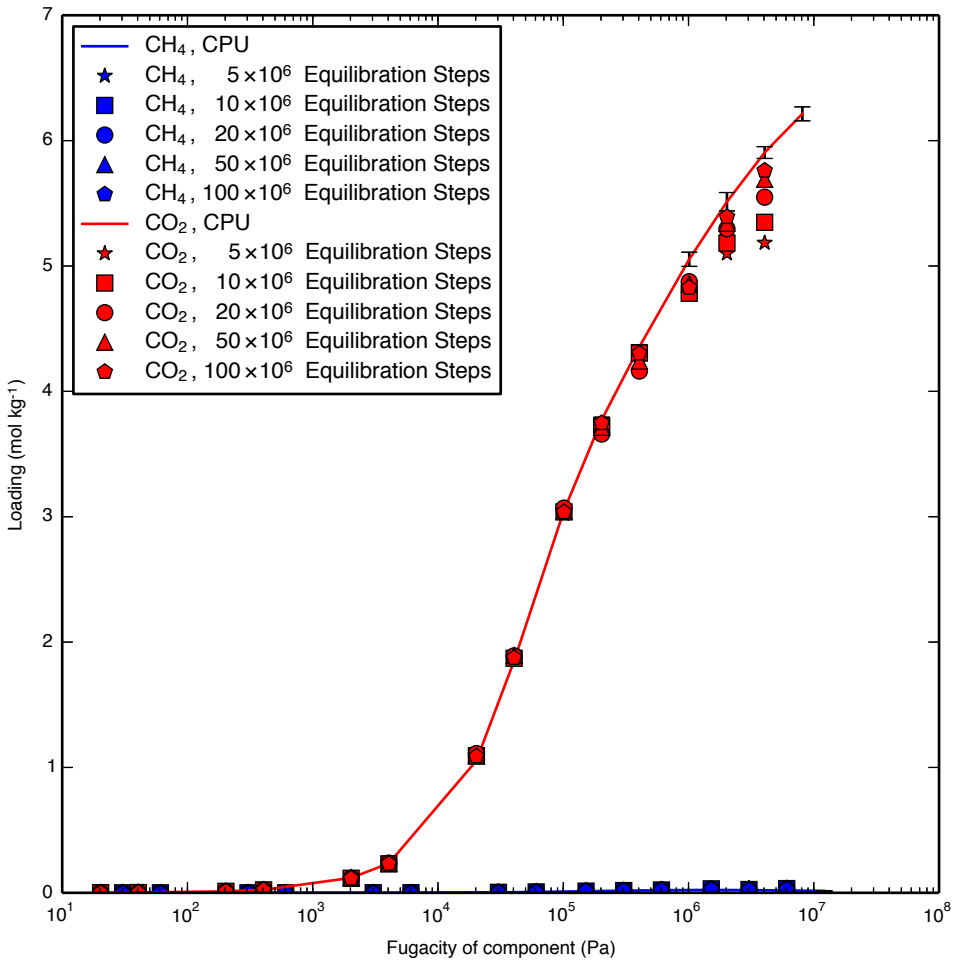

Fig. S24: Mixture isotherms of CH_4 (60 mol %) and CO_2 (40 mol %) in the IZA zeolite ABW, used to verify the GPU code. Unlike the isotherms used in the screening, these used the ideal gas equation of state and no pocket blocking. The CPU data were computed using 200,000 equilibration cycles and 100,000 production cycles, with error bars presented. The remainder of the data were generated using the GPU code with varying numbers of equilibration steps and 1,000,000 production steps.

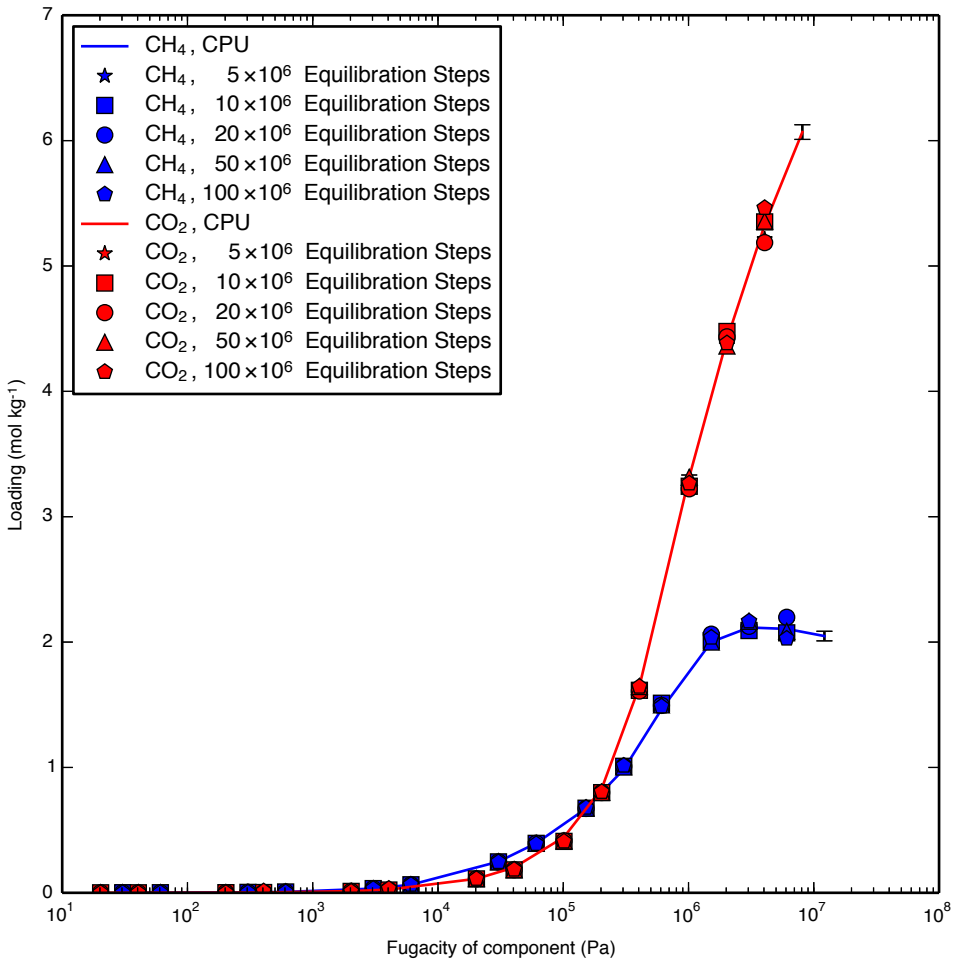

Fig. S25: Mixture isotherms of CH_4 (60 mol %) and CO_2 (40 mol %) in the IZA zeolite FAU, used to verify the GPU code. Unlike the isotherms used in the screening, these used the ideal gas equation of state and no pocket blocking. The CPU data were computed using 200,000 equilibration cycles and 100,000 production cycles, with error bars presented. The remainder of the data were generated using the GPU code with varying numbers of equilibration steps and 1,000,000 production steps.

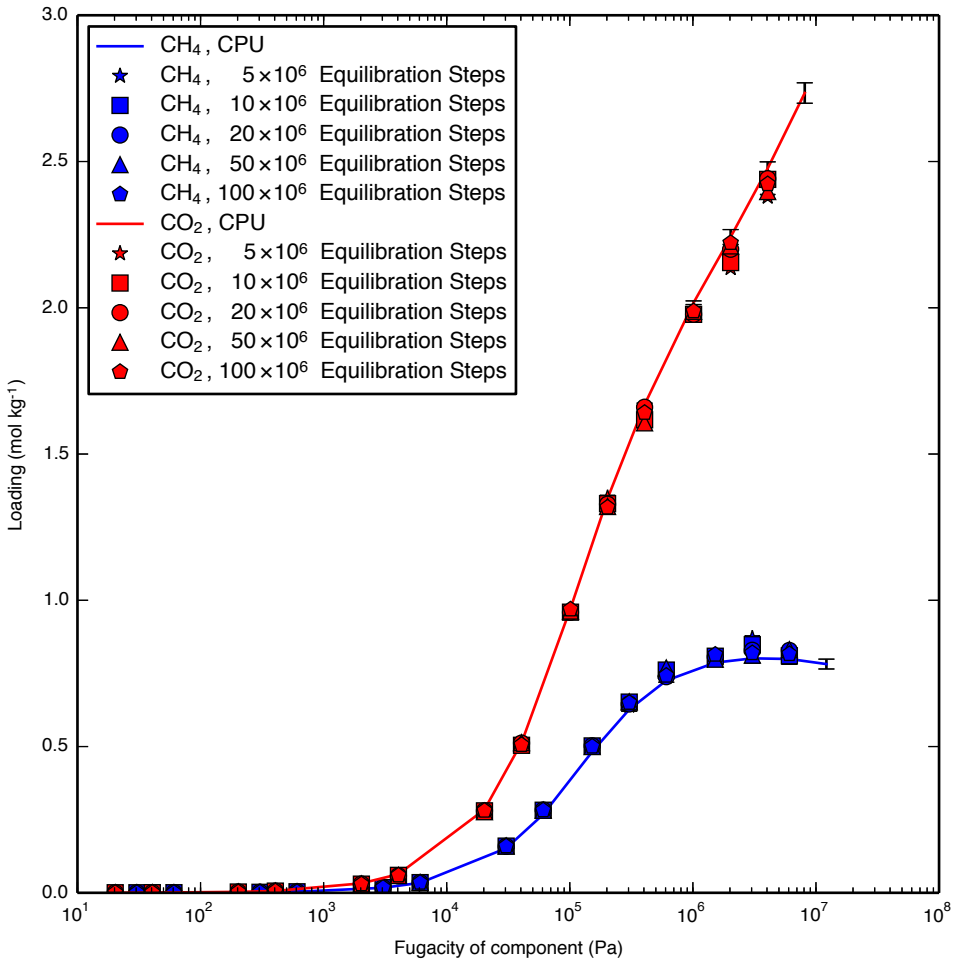

Fig. S26: Mixture isotherms of CH_4 (60 mol %) and CO_2 (40 mol %) in the IZA zeolite MFI, used to verify the GPU code. Unlike the isotherms used in the screening, these used the ideal gas equation of state and no pocket blocking. The CPU data were computed using 200,000 equilibration cycles and 100,000 production cycles, with error bars presented. The remainder of the data were generated using the GPU code with varying numbers of equilibration steps and 1,000,000 production steps.

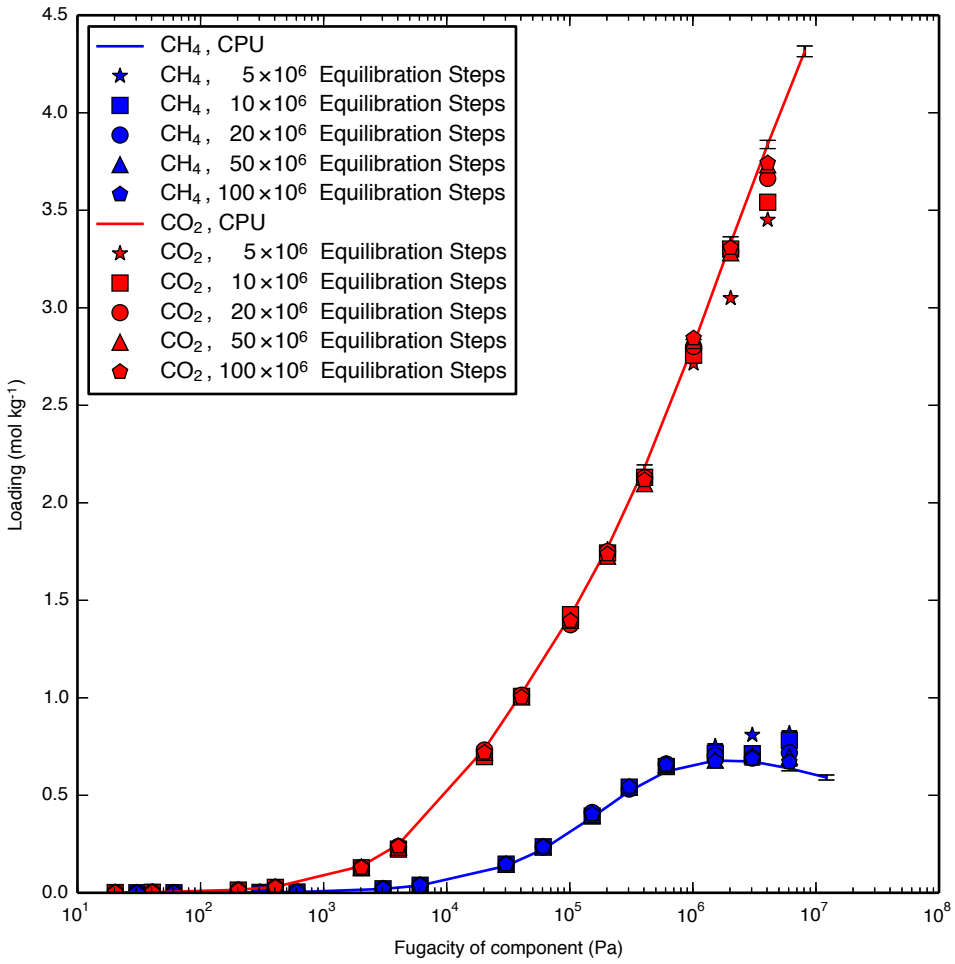

Fig. S27: Mixture isotherms of CH_4 (60 mol %) and CO_2 (40 mol %) in the IZA zeolite MOR, used to verify the GPU code. Unlike the isotherms used in the screening, these used the ideal gas equation of state and no pocket blocking. The CPU data were computed using 200,000 equilibration cycles and 100,000 production cycles, with error bars presented. The remainder of the data were generated using the GPU code with varying numbers of equilibration steps and 1,000,000 production steps.

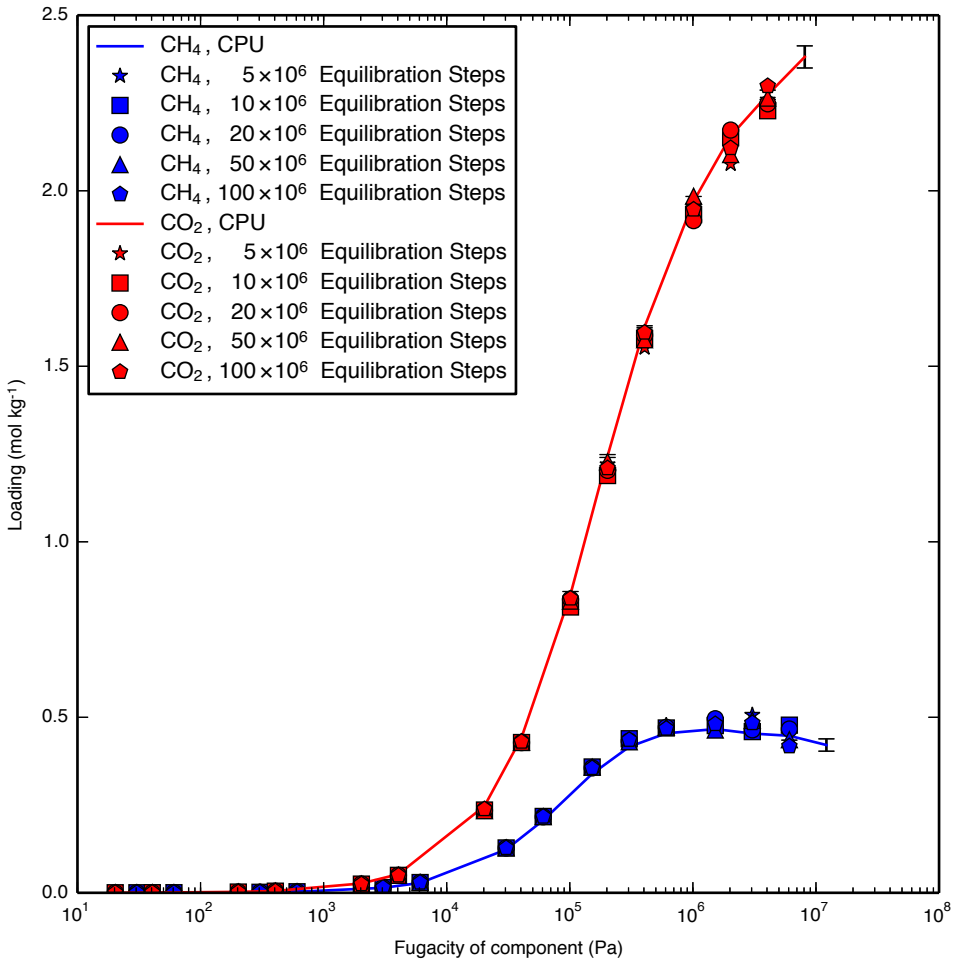

Fig. S28: Mixture isotherms of CH_4 (60 mol %) and CO_2 (40 mol %) in the IZA zeolite TON, used to verify the GPU code. Unlike the isotherms used in the screening, these used the ideal gas equation of state and no pocket blocking. The CPU data were computed using 200,000 equilibration cycles and 100,000 production cycles, with error bars presented. The remainder of the data were generated using the GPU code with varying numbers of equilibration steps and 1,000,000 production steps.

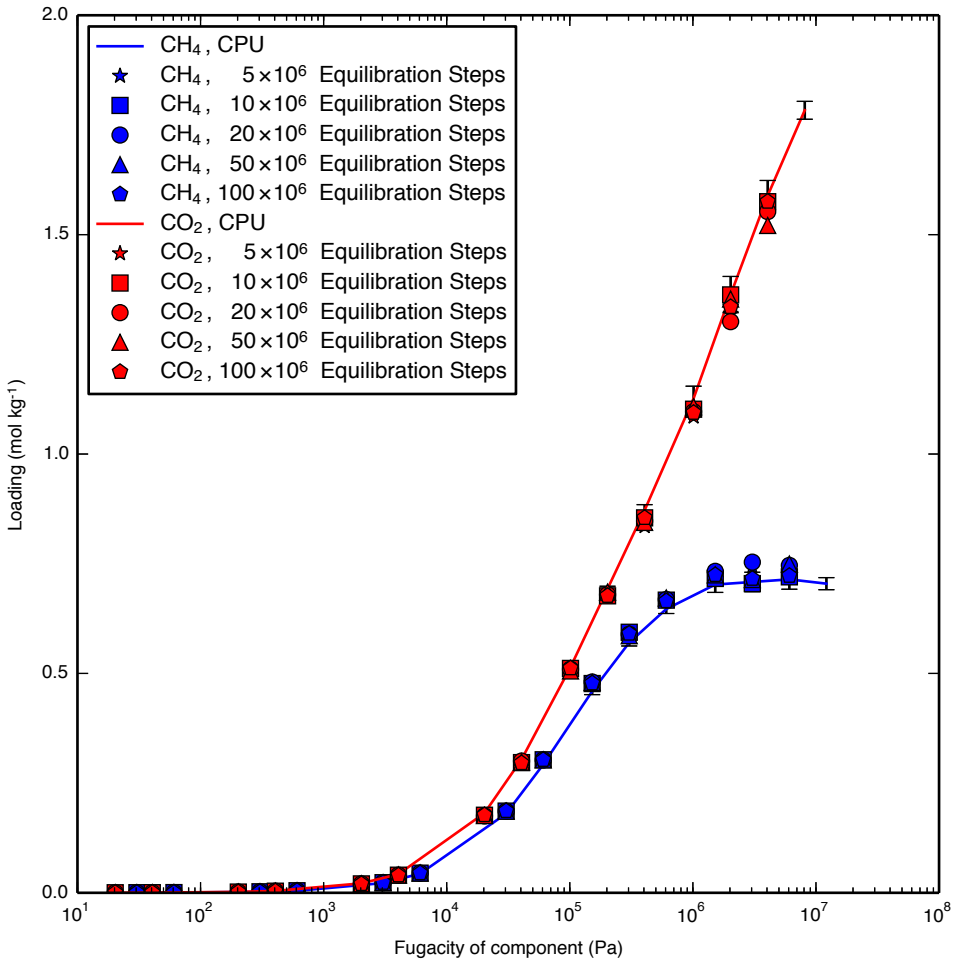

Fig. S29: Mixture isotherms of CH_4 (60 mol %) and CO_2 (40 mol %) in the hypothetical zeolite PCOD8170391, used to verify the GPU code. Unlike the isotherms used in the screening, these used the ideal gas equation of state and no pocket blocking. The CPU data were computed using 200,000 equilibration cycles and 100,000 production cycles, with error bars presented. The remainder of the data were generated using the GPU code with varying numbers of equilibration steps and 1,000,000 production steps.

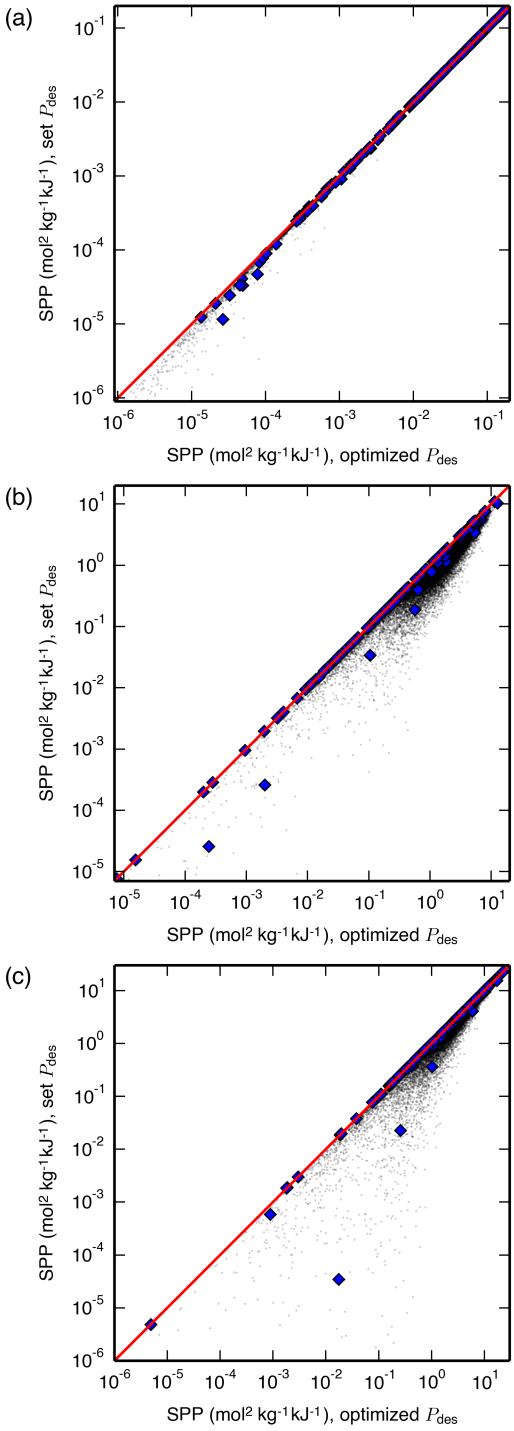

Fig. S30: A correlation between the SPP of materials evaluated at a set desorption pressure and the SPP evaluated at each material's optimal desorption pressure for the (a) LFG, (b) APG, and (c) NAG processes undergoing PSA. The LFG process used a set desorption pressure of 0.1 bar and the APG and NAG processes used a set desorption pressure of 1 bar, which might have been suspected as near-optimal desorption pressures for these processes prior to completing the present study.[20] Hypothetical zeolites are shown as black dots, and IZA zeolites are shown as blue diamonds. A line is drawn at $y = x$ for reference.

4 Supplementary Tables

All data in the following tables were taken from the analysis of PSA processes. Therefore all desorption temperatures are 300 K and all sensible energies are $0\,\mathrm{kJ\,mol^{-1}}$.

Zeolites AST, LTN, MEP, NON, SGT, and UOZ were found to have a negative $Q_{\mathrm{st,CO_2}}$ and thus could not be used for any separations, so they are not included in the tables. In addition, some zeolites had a positive $Q_{\mathrm{st,CO_2}}$ but were found to have a required mass of adsorbent that was negative for a particular separation; this meant that they were unsuitable for that separation, and so they are not included in the tables. These include the zeolites GON, MRE, and SAF for the LFG PSA process, the zeolite MRE for the APG PSA process, and the zeolites ATV, BOF, and MRE for the NAG PSA process.

Table S1: Results of the LFG process carried out with PSA

Ads.	P_{des} (kPa)	$\Delta q_{\mathrm{CH_4}}$ $\left(\mathrm{mol\,kg^{-1}}\right)$	$\Delta q_{\mathrm{CO_2}}$ $\left(\mathrm{mol\,kg^{-1}}\right)$	$\frac{M_{\mathrm{ads}}}{M_{\mathrm{CH_4,raff}}} \sum_{i=1}^{2} \left[\Delta q_i Q_{\mathrm{st},i}\right]$ $\left(\mathrm{kJ\,mol^{-1}}\right)$	$\frac{W_{\mathrm{vac}}}{M_{\mathrm{CH_4,raff}}}$ $\left(\mathrm{kJ\,mol^{-1}}\right)$	$\frac{E}{M_{\mathrm{CH_4,raff}}}$ $\left(\mathrm{kJ\,mol^{-1}}\right)$	$\frac{M_{\mathrm{ads}}}{M_{\mathrm{CH_4,raff}}}$ $\left(\mathrm{kg\,mol^{-1}}\right)$	$\frac{M_{\mathrm{CH_4,raff}}}{M_{\mathrm{CH_4,feed}}}$	SPP $\left(\mathrm{mol^2\,kg^{-1}\,kJ^{-1}}\right)$
WEI	10.0	<0.01	3.52	25.10	6.54	31.64	0.18	1.00	1.72×10^{-1}
MON	11.2	0.01	2.60	21.51	6.19	27.70	0.25	1.00	1.44×10^{-1}
GIS	10.0	0.08	2.34	21.79	6.90	28.69	0.28	0.98	1.21×10^{-1}
SIV	10.0	0.09	2.01	21.65	7.03	28.68	0.33	0.97	1.02×10^{-1}
ABW	10.0	0.01	1.62	20.42	6.57	27.00	0.40	1.00	9.26×10^{-2}
APC	10.1	0.00	1.56	20.91	6.50	27.41	0.41	1.00	8.80×10^{-2}
PHI	10.3	0.11	1.66	21.41	7.14	28.55	0.41	0.96	8.26×10^{-2}
RWR	10.0	0.00	1.46	21.57	6.53	28.10	0.44	1.00	8.02×10^{-2}
AHT	10.0	0.00	1.41	22.88	6.53	29.41	0.46	1.00	7.44×10^{-2}
JBW	10.0	0.01	1.43	23.59	6.59	30.18	0.45	1.00	7.29×10^{-2}
BIK	10.0	<0.01	1.22	21.22	6.57	27.79	0.53	1.00	6.75×10^{-2}
MER	10.0	0.12	1.42	21.93	7.48	29.41	0.48	0.95	6.71×10^{-2}
ATN	10.0	0.10	1.39	22.85	7.31	30.16	0.49	0.96	6.52×10^{-2}
SOD	10.4	0.00	0.92	17.19	6.38	23.57	0.70	1.00	6.05×10^{-2}
MVY	10.0	0.00	1.20	25.21	6.53	31.74	0.54	1.00	5.86×10^{-2}
PAU	10.3	0.16	1.34	22.44	7.79	30.23	0.52	0.92	5.82×10^{-2}
LOV	10.0	0.13	1.36	25.09	7.64	32.73	0.51	0.94	5.66×10^{-2}
DFT	10.0	0.30	1.72	28.63	8.69	37.32	0.43	0.89	5.59×10^{-2}
AEN	10.0	0.01	1.00	20.87	6.62	27.49	0.65	0.99	5.58×10^{-2}
PUN	13.0	0.21	1.21	22.41	7.45	29.85	0.60	0.89	4.93×10^{-2}
ATT	10.0	0.20	1.24	24.19	8.49	32.68	0.58	0.90	4.71×10^{-2}
KFI	13.0	0.15	1.02	21.38	7.10	28.48	0.70	0.91	4.55×10^{-2}
CAS	10.0	0.00	0.78	20.13	6.53	26.67	0.83	1.00	4.54×10^{-2}
VSV	14.0	0.02	0.76	19.47	5.60	25.07	0.87	0.98	4.53×10^{-2}
NAB	12.9	<0.01	0.68	17.60	5.71	23.31	0.95	1.00	4.47×10^{-2}
RHO	10.0	0.22	1.19	26.25	8.84	35.09	0.62	0.88	4.06×10^{-2}
GOO	10.2	0.00	0.56	18.55	6.47	25.03	1.15	1.00	3.47×10^{-2}
UEI	10.0	0.13	0.92	25.75	8.25	34.00	0.78	0.91	3.43×10^{-2}
AWO	10.0	0.13	0.82	28.09	8.43	36.52	0.88	0.90	2.81×10^{-2}
ACO	11.2	0.07	0.57	21.43	7.44	28.87	1.23	0.92	2.61×10^{-2}
ASV	11.8	0.17	0.76	24.85	8.50	33.35	1.00	0.86	2.58×10^{-2}
TSC	10.0	0.10	0.70	27.68	8.27	35.94	1.01	0.91	2.49×10^{-2}
EON	10.0	0.10	0.69	27.41	8.22	35.63	1.04	0.91	2.46×10^{-2}
ATS	15.0	0.12	0.59	20.86	7.12	27.97	1.27	0.87	2.44×10^{-2}
SAV	15.1	0.18	0.64	23.19	7.94	31.13	1.23	0.82	2.14×10^{-2}
MOR	10.0	0.19	0.77	30.89	9.73	40.62	1.00	0.84	2.07×10^{-2}
SOS	14.9	0.05	0.35	18.18	6.54	24.72	2.02	0.90	1.81×10^{-2}
JRY	10.8	0.15	0.59	25.13	9.52	34.65	1.33	0.83	1.80×10^{-2}
OWE	17.4	0.26	0.71	29.68	8.30	37.99	1.20	0.76	1.68×10^{-2}
SSY	16.1	0.10	0.40	20.92	7.26	28.18	1.95	0.84	1.53×10^{-2}
APD	10.0	0.28	0.75	34.66	11.82	46.48	1.14	0.76	1.44×10^{-2}
VNI	14.5	0.00	0.21	17.24	5.23	22.47	3.09	1.00	1.44×10^{-2}
SZR	14.9	0.16	0.51	27.12	8.67	35.79	1.63	0.79	1.35×10^{-2}
MTN	14.0	0.00	0.14	12.96	5.34	18.31	4.49	1.00	1.22×10^{-2}
AEI	19.1	0.21	0.52	26.58	8.43	35.01	1.72	0.73	1.21×10^{-2}
SFH	16.2	0.08	0.30	21.27	7.56	28.83	2.67	0.82	1.07×10^{-2}
PON	13.7	0.18	0.46	28.89	10.06	38.95	1.90	0.75	1.01×10^{-2}
NAT	13.7	0.12	0.35	24.56	9.34	33.90	2.40	0.78	9.58×10^{-3}
MTT	14.5	0.14	0.38	27.00	9.59	36.59	2.27	0.75	9.10×10^{-3}
MFS	16.1	0.18	0.44	30.07	9.65	39.71	2.06	0.72	8.86×10^{-3}
CGS	18.4	0.21	0.41	32.91	10.00	42.92	2.35	0.67	6.68×10^{-3}
SBE	10.5	0.16	0.36	31.85	12.87	44.71	2.53	0.72	6.32×10^{-3}
AFR	15.5	0.15	0.32	28.88	10.51	39.38	2.90	0.70	6.15×10^{-3}
UFI	15.9	0.29	0.51	41.71	12.35	54.06	2.03	0.63	5.74×10^{-3}
TON	16.8	0.17	0.34	31.79	10.52	42.31	2.81	0.68	5.72×10^{-3}
OBW	20.7	0.19	0.35	30.32	9.85	40.17	2.93	0.65	5.48×10^{-3}
MFI	13.6	0.23	0.42	37.74	13.48	51.23	2.46	0.64	5.04×10^{-3}
STI	20.5	0.25	0.40	37.06	11.17	48.22	2.71	0.60	4.59×10^{-3}
TER	13.9	0.27	0.41	40.74	15.83	56.56	2.83	0.57	3.56×10^{-3}
ITE	24.6	0.20	0.31	37.06	10.30	47.36	3.67	0.58	3.31×10^{-3}
AWW	26.4	0.21	0.31	44.35	10.29	54.64	3.82	0.55	2.66×10^{-3}
LTA	20.2	0.14	0.22	33.70	11.59	45.30	5.09	0.59	2.57×10^{-3}
ITR	21.5	0.19	0.27	41.93	12.46	54.39	4.38	0.55	2.29×10^{-3}
SAS	17.7	0.20	0.28	42.70	15.26	57.96	4.54	0.52	1.99×10^{-3}
ITH	18.8	0.20	0.27	46.65	15.46	62.11	4.78	0.51	1.70×10^{-3}
IWV	19.8	0.11	0.16	33.02	12.92	45.94	7.34	0.56	1.65×10^{-3}
NES	18.8	0.17	0.22	42.97	15.57	58.54	5.90	0.50	1.46×10^{-3}
BOF	10.0	0.34	0.41	61.01	27.14	88.15	3.59	0.45	1.42×10^{-3}
IHW	23.2	0.16	0.22	48.22	13.17	61.39	5.96	0.51	1.38×10^{-3}
ATV	10.0	0.19	0.25	59.50	23.49	82.99	5.24	0.50	1.15×10^{-3}
ESV	28.8	0.22	0.26	62.44	12.93	75.36	5.62	0.45	1.06×10^{-3}
MSE	22.3	0.19	0.22	53.81	16.69	70.50	6.93	0.44	8.93×10^{-4}
OSI	22.4	0.09	0.12	41.55	13.49	55.04	10.40	0.51	8.85×10^{-4}
UOS	14.8	0.22	0.25	63.12	23.48	86.60	6.24	0.42	7.79×10^{-4}
THO	11.8	0.30	0.32	74.24	30.80	105.04	5.36	0.38	6.77×10^{-4}
MEL	19.2	0.25	0.26	68.59	22.58	91.17	6.59	0.38	6.30×10^{-4}
IWR	20.9	0.20	0.21	59.45	21.05	80.50	8.28	0.38	5.72×10^{-4}
CFI	23.9	0.07	0.09	41.76	14.09	55.85	14.88	0.47	5.70×10^{-4}
EUO	21.4	0.16	0.18	59.91	19.14	79.05	9.03	0.40	5.66×10^{-4}
FAU	25.4	0.08	0.09	38.73	15.58	54.31	17.91	0.42	4.37×10^{-4}
ANA	12.9	0.00	0.01	17.36	5.63	22.98	112.21	1.00	3.88×10^{-4}
IWW	24.3	0.18	0.18	69.34	20.92	90.27	10.57	0.35	3.65×10^{-4}
BOG	18.6	0.18	0.18	68.44	26.33	94.77	10.53	0.34	3.43×10^{-4}
RWY	24.6	0.10	0.10	42.84	20.54	63.38	18.87	0.35	2.94×10^{-4}
EDI	12.0	0.40	0.37	115.09	43.92	159.01	6.25	0.29	2.87×10^{-4}
SFG	20.7	0.15	0.15	74.77	24.83	99.60	12.85	0.34	2.63×10^{-4}
IWS	32.4	0.12	0.11	74.69	20.92	95.61	21.35	0.28	1.38×10^{-4}
ZON	25.0	0.32	0.27	155.60	36.10	191.70	11.20	0.22	1.01×10^{-4}
SAO	28.3	0.13	0.12	84.57	28.41	112.98	23.49	0.24	9.16×10^{-5}
ISV	31.0	0.15	0.13	98.01	27.56	125.57	22.35	0.23	8.26×10^{-5}
FER	36.1	0.27	0.22	157.76	26.95	184.71	14.39	0.21	7.77×10^{-5}
BEA	69.1	0.07	0.06	97.02	7.73	104.75	45.81	0.24	4.94×10^{-5}
AET	27.6	0.05	0.04	73.81	25.65	99.46	57.22	0.27	4.75×10^{-5}
CDO	38.7	0.20	0.16	175.05	26.72	201.77	21.30	0.19	4.51×10^{-5}
VET	39.8	0.07	0.06	114.83	21.79	136.62	50.35	0.22	3.27×10^{-5}
EZT	71.8	0.07	0.06	131.05	8.09	139.13	55.82	0.21	2.66×10^{-5}
AFO	25.7	0.17	0.13	192.82	50.07	242.89	31.14	0.16	2.11×10^{-5}
BCT	24.0	0.00	<0.01	8.32	3.63	11.96	6,238.17	1.00	1.34×10^{-5}
BEC	89.1	0.02	0.02	230.78	5.65	236.43	360.28	0.11	1.25×10^{-6}
AEL	70.7	0.06	0.04	396.98	23.20	420.18	196.81	0.08	9.90×10^{-7}
DON	99.7	<0.01	<0.01	32,946.12	27.61	32,973.72	5,349,761.05	<0.01	3.87×10^{-15}

Table S2: Results of the APG process carried out with PSA

Ads.	P_{des} (kPa)	$\Delta q_{\mathrm{CH_4}}$ $\left(\mathrm{mol\,kg^{-1}}\right)$	$\Delta q_{\mathrm{CO_2}}$ $\left(\mathrm{mol\,kg^{-1}}\right)$	$\frac{M_{\mathrm{ads}}}{M_{\mathrm{CH_4,raff}}} \sum_{i=1}^{2} \left[\Delta q_i Q_{\mathrm{st},i}\right]$ $\left(\mathrm{kJ\,mol^{-1}}\right)$	$\frac{W_{\mathrm{vac}}}{M_{\mathrm{CH_4,raff}}}$ $\left(\mathrm{kJ\,mol^{-1}}\right)$	$\frac{E}{M_{\mathrm{CH_4,raff}}}$ $\left(\mathrm{kJ\,mol^{-1}}\right)$	$\frac{M_{\mathrm{ads}}}{M_{\mathrm{CH_4,raff}}}$ $\left(\mathrm{kg\,mol^{-1}}\right)$	$\frac{M_{\mathrm{CH_4,raff}}}{M_{\mathrm{CH_4,feed}}}$	SPP $\left(\mathrm{mol^2\,kg^{-1}\,kJ^{-1}}\right)$
WEI	23.6	0.02	4.69	3.53	0.52	4.05	0.02	1.00	1.28×10^{1}
MON	52.7	0.12	3.43	3.06	0.22	3.28	0.03	1.00	1.14×10^{1}
APC	48.5	0.00	2.28	2.93	0.24	3.17	0.04	1.00	7.93×10^{0}
ABW	46.5	0.06	2.28	2.90	0.26	3.16	0.04	1.00	7.91×10^{0}
GIS	24.4	0.53	2.62	3.38	0.62	3.99	0.04	0.98	6.93×10^{0}
RWR	34.6	0.00	2.01	3.03	0.36	3.39	0.05	1.00	6.53×10^{0}
SIV	33.4	0.53	2.26	3.39	0.48	3.87	0.04	0.98	6.13×10^{0}
AHT	34.0	0.00	1.85	3.21	0.37	3.58	0.05	1.00	5.71×10^{0}
SOD	50.4	0.00	1.31	2.41	0.22	2.64	0.07	1.00	5.49×10^{0}
JBW	13.8	0.06	2.04	3.35	0.78	4.13	0.04	1.00	5.41×10^{0}
BIK	32.2	0.04	1.62	3.01	0.40	3.41	0.06	1.00	5.23×10^{0}
VSV	90.6	0.21	1.41	2.91	0.04	2.94	0.07	0.99	5.14×10^{0}
NAB	80.8	0.05	1.20	2.52	0.07	2.59	0.08	1.00	5.09×10^{0}
PHI	45.9	0.58	1.85	3.45	0.35	3.80	0.05	0.97	5.02×10^{0}
AEN	46.6	0.07	1.40	2.99	0.27	3.26	0.06	1.00	4.71×10^{0}
MVY	29.8	0.00	1.66	3.54	0.42	3.96	0.05	1.00	4.63×10^{0}
CAS	46.3	0.00	1.15	2.83	0.25	3.08	0.08	1.00	4.12×10^{0}
MER	46.6	0.64	1.53	3.69	0.38	4.07	0.06	0.96	3.80×10^{0}
PAU	51.2	0.88	1.55	3.92	0.37	4.28	0.06	0.95	3.54×10^{0}
LOV	51.0	0.66	1.56	4.19	0.33	4.52	0.06	0.96	3.48×10^{0}
GOO	51.5	0.00	0.84	2.60	0.22	2.82	0.11	1.00	3.28×10^{0}
PUN	81.9	1.09	1.44	4.06	0.12	4.18	0.07	0.93	3.23×10^{0}
ATN	25.1	0.47	1.35	3.76	0.69	4.45	0.07	0.97	3.11×10^{0}
KFI	79.7	0.86	1.25	3.82	0.13	3.94	0.08	0.94	3.01×10^{0}
ATS	100.0	0.69	0.79	3.80	0.00	3.80	0.13	0.92	1.91×10^{0}
DFT	15.2	1.63	1.59	6.04	1.63	7.66	0.06	0.91	1.84×10^{0}
RHO	29.4	1.66	1.39	5.64	1.08	6.72	0.07	0.89	1.76×10^{0}
SAV	100.0	0.98	0.87	4.46	0.00	4.46	0.12	0.90	1.68×10^{0}
VNI	73.1	0.00	0.36	2.42	0.10	2.52	0.25	1.00	1.58×10^{0}
EON	24.8	0.62	0.92	4.81	0.90	5.71	0.11	0.94	1.54×10^{0}
ATT	27.2	1.02	1.05	5.19	1.01	6.20	0.10	0.91	1.52×10^{0}
SOS	100.0	0.39	0.54	3.47	0.00	3.47	0.18	0.93	1.47×10^{0}
ACO	50.2	0.76	0.80	4.63	0.49	5.12	0.13	0.91	1.41×10^{0}
TSC	30.9	0.97	0.93	5.09	0.94	6.03	0.11	0.90	1.35×10^{0}
MTN	83.2	0.00	0.23	1.82	0.06	1.88	0.40	1.00	1.33×10^{0}
SSY	100.0	0.58	0.55	4.01	0.00	4.01	0.19	0.90	1.21×10^{0}
SZR	100.0	0.65	0.63	4.71	0.00	4.71	0.16	0.90	1.18×10^{0}
AEI	100.0	1.08	0.73	5.13	0.00	5.13	0.15	0.86	1.14×10^{0}
UEI	18.2	0.98	0.90	5.84	1.50	7.34	0.11	0.90	1.06×10^{0}
SFH	100.0	0.60	0.46	4.35	0.00	4.35	0.23	0.88	8.71×10^{-1}
MFS	100.0	0.76	0.50	5.77	0.00	5.77	0.22	0.86	6.91×10^{-1}
ASV	57.6	0.66	0.51	5.95	0.48	6.43	0.21	0.88	6.57×10^{-1}
MOR	15.4	1.14	0.76	7.30	2.11	9.41	0.14	0.86	6.41×10^{-1}
JRY	45.1	0.93	0.60	6.45	0.82	7.27	0.18	0.85	6.41×10^{-1}
AFR	100.0	1.10	0.55	6.35	0.00	6.35	0.21	0.81	5.99×10^{-1}
OWE	100.0	0.71	0.47	6.36	0.00	6.36	0.23	0.86	5.91×10^{-1}
AWO	10.0	1.12	0.75	7.60	2.75	10.35	0.15	0.86	5.72×10^{-1}
NAT	79.4	0.97	0.48	7.14	0.28	7.42	0.25	0.81	4.42×10^{-1}
OBW	100.0	1.35	0.54	7.79	0.00	7.79	0.23	0.76	4.18×10^{-1}
MTT	90.1	0.50	0.31	6.06	0.10	6.16	0.36	0.85	3.85×10^{-1}
AWW	100.0	0.61	0.32	6.93	0.00	6.93	0.36	0.82	3.32×10^{-1}
ITE	100.0	1.17	0.45	8.15	0.00	8.15	0.28	0.75	3.32×10^{-1}
CGS	100.0	0.80	0.36	8.20	0.00	8.20	0.34	0.79	2.85×10^{-1}
PON	51.0	1.06	0.45	9.24	1.01	10.25	0.28	0.77	2.72×10^{-1}
LTA	100.0	1.11	0.39	8.05	0.00	8.05	0.34	0.73	2.66×10^{-1}
SBE	34.9	1.13	0.44	9.43	1.81	11.25	0.29	0.75	2.29×10^{-1}
SAS	100.0	1.06	0.37	8.98	0.00	8.98	0.36	0.72	2.23×10^{-1}
TON	89.3	0.67	0.29	8.33	0.16	8.49	0.42	0.78	2.18×10^{-1}
MFI	88.3	0.94	0.35	10.27	0.20	10.47	0.37	0.74	1.89×10^{-1}
UFI	95.1	1.14	0.41	11.92	0.08	12.00	0.32	0.73	1.88×10^{-1}
STI	100.0	0.93	0.33	9.86	0.00	9.86	0.40	0.73	1.85×10^{-1}
ITR	100.0	0.84	0.29	9.91	0.00	9.91	0.46	0.72	1.60×10^{-1}
IWV	100.0	1.00	0.29	9.66	0.00	9.66	0.51	0.66	1.34×10^{-1}
ESV	100.0	0.55	0.22	9.98	0.00	9.98	0.58	0.76	1.30×10^{-1}
ITH	100.0	0.86	0.27	11.28	0.00	11.28	0.52	0.69	1.19×10^{-1}
APD	10.3	2.20	0.61	17.75	6.95	24.70	0.25	0.65	1.05×10^{-1}
TER	62.5	1.28	0.36	13.70	1.15	14.85	0.42	0.65	1.03×10^{-1}
NES	100.0	0.88	0.25	11.31	0.00	11.31	0.58	0.66	1.00×10^{-1}
IHW	100.0	0.58	0.20	10.53	0.00	10.54	0.69	0.71	9.88×10^{-2}
MSE	100.0	0.98	0.27	12.16	0.00	12.16	0.56	0.65	9.46×10^{-2}
OSI	100.0	0.48	0.16	9.13	0.00	9.13	0.83	0.71	9.45×10^{-2}
CFI	100.0	0.56	0.16	10.26	0.00	10.26	0.95	0.65	6.67×10^{-2}
EUO	100.0	0.74	0.20	13.55	0.00	13.55	0.79	0.63	5.90×10^{-2}
IWR	100.0	1.17	0.26	16.01	0.00	16.01	0.67	0.56	5.18×10^{-2}
ANA	69.9	0.00	0.01	2.44	0.11	2.55	8.74	1.00	4.49×10^{-2}
FAU	100.0	0.86	0.18	13.31	0.00	13.31	1.07	0.52	3.65×10^{-2}
IWW	100.0	0.97	0.21	18.22	0.00	18.22	0.89	0.54	3.32×10^{-2}
BOG	100.0	1.13	0.23	19.06	0.00	19.06	0.83	0.52	3.25×10^{-2}
MEL	100.0	1.02	0.22	20.63	0.00	20.63	0.87	0.53	2.97×10^{-2}
UOS	83.7	1.05	0.22	21.80	0.65	22.45	0.84	0.53	2.82×10^{-2}
FER	100.0	0.94	0.21	22.25	0.00	22.25	0.89	0.54	2.73×10^{-2}
RWY	100.0	1.15	0.20	16.46	0.00	16.47	1.18	0.42	2.17×10^{-2}
IWS	100.0	1.03	0.20	19.67	0.00	19.67	1.10	0.47	2.16×10^{-2}
SAO	100.0	1.19	0.21	21.13	0.00	21.13	1.10	0.43	1.87×10^{-2}
THO	61.2	1.57	0.29	32.06	2.63	34.69	0.82	0.44	1.54×10^{-2}
ISV	100.0	1.13	0.20	24.74	0.00	24.74	1.23	0.42	1.38×10^{-2}
SFG	100.0	0.76	0.14	25.47	0.00	25.47	1.57	0.46	1.14×10^{-2}
BEA	100.0	1.18	0.20	28.06	0.00	28.06	1.31	0.39	1.07×10^{-2}
AET	100.0	0.46	0.09	18.97	0.00	18.97	2.59	0.46	9.30×10^{-3}
VET	100.0	0.40	0.08	23.86	0.00	23.86	2.88	0.46	6.76×10^{-3}
EZT	100.0	0.98	0.15	41.29	0.00	41.30	2.02	0.34	4.03×10^{-3}
CDO	100.0	0.75	0.12	42.92	0.00	42.92	2.21	0.38	3.95×10^{-3}
BEC	100.0	1.14	0.17	41.59	0.00	41.59	2.06	0.30	3.50×10^{-3}
ZON	100.0	0.79	0.13	48.01	0.00	48.01	2.31	0.36	3.20×10^{-3}
BOF	10.0	1.71	0.25	63.32	29.78	93.10	1.50	0.28	2.00×10^{-3}
BCT	100.0	0.00	<0.01	1.17	0.00	1.17	436.28	1.00	1.96×10^{-3}
AFO	96.1	0.64	0.09	63.37	0.42	63.79	4.35	0.26	9.54×10^{-4}
SAF	100.0	0.57	0.08	81.51	0.00	81.51	7.86	0.18	2.83×10^{-4}
EDI	10.0	2.10	0.27	147.41	66.69	214.11	2.79	0.15	2.44×10^{-4}
DON	100.0	0.60	0.08	82.74	0.00	82.74	9.23	0.15	1.99×10^{-4}
ATV	10.0	1.51	0.19	191.63	82.13	273.76	4.79	0.12	9.27×10^{-5}
GON	100.0	0.57	0.07	238.50	0.00	238.50	20.98	0.08	1.55×10^{-5}
AEL	95.5	0.66	0.08	343.77	2.64	346.41	23.18	0.06	7.69×10^{-6}

Table S3: Results of the NAG process carried out with PSA

Ads.	P_{des} (kPa)	$\Delta q_{\mathrm{CH_4}}$ $\left(\mathrm{mol\,kg^{-1}}\right)$	$\Delta q_{\mathrm{CO_2}}$ $\left(\mathrm{mol\,kg^{-1}}\right)$	$\frac{M_{\mathrm{ads}}}{M_{\mathrm{CH_4,raff}}} \sum_{i=1}^{2} \left[\Delta q_i Q_{\mathrm{st},i}\right]$ $\left(\mathrm{kJ\,mol^{-1}}\right)$	$\frac{W_{\mathrm{vac}}}{M_{\mathrm{CH_4,raff}}}$ $\left(\mathrm{kJ\,mol^{-1}}\right)$	$\frac{E}{M_{\mathrm{CH_4,raff}}}$ $\left(\mathrm{kJ\,mol^{-1}}\right)$	$\frac{M_{\mathrm{ads}}}{M_{\mathrm{CH_4,raff}}}$ $\left(\mathrm{kg\,mol^{-1}}\right)$	$\frac{M_{\mathrm{CH_4,raff}}}{M_{\mathrm{CH_4,feed}}}$	SPP $\left(\mathrm{mol^2\,kg^{-1}\,kJ^{-1}}\right)$
NAB	100.0	0.28	5.27	2.53	0.00	2.53	0.02	1.00	2.27×10^{1}
VSV	100.0	0.70	4.80	2.90	0.00	2.90	0.02	0.99	1.77×10^{1}
WEI	29.8	0.03	6.17	3.53	0.42	3.95	0.01	1.00	1.72×10^{1}
MON	66.2	0.40	4.91	3.15	0.14	3.29	0.02	0.99	1.62×10^{1}
ABW	75.8	0.16	3.92	2.92	0.09	3.01	0.02	1.00	1.43×10^{1}
APC	77.2	0.00	3.60	2.93	0.08	3.01	0.03	1.00	1.32×10^{1}
PUN	100.0	1.38	3.81	3.21	0.00	3.21	0.02	0.97	1.21×10^{1}
SOD	100.0	0.00	2.61	2.41	0.00	2.41	0.03	1.00	1.19×10^{1}
PHI	100.0	0.63	3.40	3.16	0.00	3.16	0.03	0.98	1.14×10^{1}
RWR	56.3	0.00	3.30	3.03	0.19	3.21	0.03	1.00	1.13×10^{1}
SIV	53.4	0.62	3.61	3.24	0.24	3.49	0.03	0.98	1.10×10^{1}
KFI	100.0	1.48	3.49	3.28	0.00	3.28	0.03	0.96	1.08×10^{1}
MER	100.0	0.63	3.13	3.20	0.00	3.20	0.03	0.98	1.03×10^{1}
GIS	34.2	0.55	3.58	3.27	0.43	3.70	0.03	0.99	1.03×10^{1}
ATN	46.0	0.00	2.95	2.93	0.26	3.18	0.03	1.00	1.02×10^{1}
VNI	100.0	0.00	2.11	2.42	0.00	2.42	0.04	1.00	9.62×10^{0}
CAS	88.4	0.00	2.19	2.83	0.04	2.86	0.04	1.00	8.42×10^{0}
SAV	100.0	1.89	2.92	3.45	0.00	3.45	0.03	0.94	8.13×10^{0}
AEN	71.2	0.15	2.27	3.03	0.11	3.14	0.04	0.99	7.86×10^{0}
GOO	100.0	0.00	1.85	2.60	0.00	2.60	0.05	1.00	7.85×10^{0}
SOS	100.0	1.08	2.30	2.96	0.00	2.96	0.04	0.96	7.78×10^{0}
AHT	43.6	0.00	2.43	3.21	0.28	3.49	0.04	1.00	7.69×10^{0}
BIK	44.3	0.11	2.32	3.05	0.29	3.34	0.04	1.00	7.59×10^{0}
ATS	100.0	1.14	2.29	3.10	0.00	3.10	0.04	0.95	7.35×10^{0}
LOV	97.3	1.20	2.98	4.14	0.01	4.16	0.03	0.96	7.27×10^{0}
PAU	100.0	1.49	2.72	3.87	0.00	3.87	0.04	0.95	6.91×10^{0}
MVY	41.4	0.00	2.38	3.54	0.30	3.83	0.04	1.00	6.83×10^{0}
JBW	15.4	0.16	2.30	3.43	0.76	4.19	0.04	0.99	5.97×10^{0}
SSY	100.0	1.06	1.81	3.12	0.00	3.12	0.05	0.95	5.67×10^{0}
AEI	100.0	2.21	2.25	3.99	0.00	3.99	0.05	0.91	5.04×10^{0}
MTN	100.0	0.00	0.83	1.82	0.00	1.82	0.11	1.00	5.03×10^{0}
SFH	100.0	1.37	1.65	3.44	0.00	3.44	0.06	0.92	4.44×10^{0}
EON	78.9	1.10	1.95	4.53	0.12	4.65	0.05	0.95	4.11×10^{0}
OBW	100.0	3.36	2.34	4.80	0.00	4.80	0.05	0.87	3.90×10^{0}
ATT	100.0	0.81	1.55	3.98	0.00	3.98	0.06	0.95	3.85×10^{0}
SZR	100.0	1.37	1.66	4.21	0.00	4.21	0.06	0.92	3.66×10^{0}
OWE	100.0	1.03	1.39	4.22	0.00	4.22	0.07	0.93	3.12×10^{0}
CGS	100.0	1.20	1.34	4.20	0.00	4.20	0.08	0.92	2.90×10^{0}
AWW	100.0	1.03	1.23	4.06	0.00	4.06	0.08	0.92	2.79×10^{0}
MFS	100.0	1.47	1.34	4.70	0.00	4.70	0.08	0.90	2.48×10^{0}
MTT	100.0	0.69	0.96	3.72	0.00	3.72	0.10	0.93	2.44×10^{0}
RHO	42.0	3.15	2.18	6.34	0.85	7.18	0.05	0.86	2.43×10^{0}
LTA	100.0	2.80	1.62	5.12	0.00	5.12	0.07	0.84	2.35×10^{0}
AFR	100.0	2.69	1.65	5.39	0.00	5.39	0.07	0.85	2.35×10^{0}
TSC	57.4	3.38	2.00	6.39	0.59	6.98	0.06	0.84	2.16×10^{0}
STI	100.0	1.45	1.15	4.85	0.00	4.85	0.09	0.88	1.98×10^{0}
UFI	100.0	2.28	1.56	6.54	0.00	6.54	0.07	0.86	1.89×10^{0}
ASV	100.0	0.76	0.90	4.63	0.00	4.63	0.11	0.92	1.80×10^{0}
ESV	100.0	0.96	0.95	4.72	0.00	4.72	0.11	0.91	1.79×10^{0}
ITE	100.0	2.45	1.36	5.86	0.00	5.86	0.08	0.83	1.70×10^{0}
SBE	100.0	3.26	1.67	7.25	0.00	7.25	0.07	0.82	1.62×10^{0}
UEI	26.2	1.40	1.24	5.95	1.15	7.10	0.08	0.90	1.51×10^{0}
SAS	100.0	2.30	1.21	6.01	0.00	6.01	0.09	0.82	1.44×10^{0}
IWV	100.0	2.92	1.18	6.53	0.00	6.53	0.11	0.76	1.10×10^{0}
OSI	100.0	1.15	0.71	5.05	0.00	5.05	0.15	0.85	1.09×10^{0}
MOR	23.2	1.80	1.19	7.33	1.58	8.91	0.09	0.86	1.06×10^{0}
DFT	10.9	2.38	1.47	8.08	2.80	10.88	0.08	0.85	1.03×10^{0}
NES	100.0	1.76	0.87	6.27	0.00	6.27	0.14	0.81	9.54×10^{-1}
NAT	100.0	2.58	1.14	7.90	0.00	7.90	0.11	0.79	9.36×10^{-1}
IHW	100.0	0.95	0.63	5.60	0.00	5.60	0.17	0.86	8.82×10^{-1}
JRY	59.7	1.62	0.90	7.22	0.58	7.80	0.13	0.83	8.46×10^{-1}
ITR	100.0	1.69	0.82	7.03	0.00	7.03	0.14	0.81	7.99×10^{-1}
CFI	100.0	1.48	0.69	5.81	0.00	5.81	0.17	0.80	7.97×10^{-1}
TON	100.0	1.22	0.68	6.61	0.00	6.61	0.17	0.83	7.52×10^{-1}
ITH	100.0	1.74	0.79	7.51	0.00	7.51	0.15	0.79	6.91×10^{-1}
FAU	100.0	3.49	1.02	7.87	0.00	7.87	0.14	0.67	5.87×10^{-1}
SAO	100.0	3.16	0.96	8.47	0.00	8.47	0.15	0.68	5.45×10^{-1}
IWR	100.0	2.39	0.84	8.54	0.00	8.54	0.16	0.73	5.43×10^{-1}
MSE	100.0	1.93	0.74	8.17	0.00	8.17	0.17	0.75	5.32×10^{-1}
IWS	100.0	2.75	0.88	8.43	0.00	8.43	0.16	0.70	5.27×10^{-1}
FER	100.0	1.44	0.66	8.43	0.00	8.43	0.18	0.79	5.16×10^{-1}
RWY	100.0	7.40	1.67	10.09	0.00	10.09	0.11	0.56	5.15×10^{-1}
MFI	100.0	1.55	0.64	9.07	0.00	9.07	0.19	0.77	4.39×10^{-1}
ACO	36.6	3.44	1.13	11.60	2.09	13.69	0.12	0.71	4.25×10^{-1}
IWW	100.0	1.91	0.67	9.10	0.00	9.11	0.20	0.72	3.99×10^{-1}
ANA	100.0	0.00	0.09	2.44	0.00	2.44	1.03	1.00	3.99×10^{-1}
PON	69.7	1.67	0.64	10.08	0.57	10.65	0.20	0.75	3.57×10^{-1}
BOG	100.0	2.40	0.74	10.22	0.00	10.22	0.19	0.69	3.50×10^{-1}
EUO	100.0	1.50	0.54	9.17	0.00	9.17	0.24	0.73	3.27×10^{-1}
CDO	100.0	1.02	0.45	8.97	0.00	8.97	0.27	0.78	3.25×10^{-1}
AWO	10.0	1.81	0.71	11.88	4.52	16.40	0.18	0.76	2.59×10^{-1}
ISV	100.0	2.55	0.68	11.31	0.00	11.31	0.23	0.63	2.44×10^{-1}
MEL	100.0	1.75	0.51	12.55	0.00	12.55	0.29	0.67	1.85×10^{-1}
THO	100.0	2.28	0.62	15.15	0.00	15.15	0.25	0.64	1.73×10^{-1}
VET	100.0	0.71	0.26	8.57	0.00	8.57	0.50	0.74	1.71×10^{-1}
TER	89.9	2.07	0.57	13.99	0.25	14.25	0.27	0.64	1.67×10^{-1}
BEA	100.0	2.57	0.62	13.42	0.00	13.42	0.27	0.59	1.64×10^{-1}
AET	100.0	1.43	0.38	9.99	0.00	9.99	0.40	0.63	1.57×10^{-1}
ZON	100.0	1.04	0.32	13.94	0.00	13.94	0.44	0.68	1.10×10^{-1}
BEC	100.0	2.52	0.54	16.79	0.00	16.79	0.35	0.53	8.89×10^{-2}
UOS	100.0	1.95	0.45	19.12	0.00	19.12	0.39	0.57	7.64×10^{-2}
SFG	100.0	1.51	0.31	20.97	0.00	20.97	0.64	0.51	3.79×10^{-2}
EZT	100.0	1.82	0.32	28.89	0.00	28.89	0.75	0.42	1.96×10^{-2}
DON	100.0	1.92	0.32	24.40	0.00	24.40	0.82	0.39	1.93×10^{-2}
BCT	100.0	0.00	<0.01	1.17	0.00	1.17	45.98	1.00	1.86×10^{-2}
APD	10.0	3.32	0.59	40.54	16.47	57.02	0.42	0.42	1.76×10^{-2}
GON	100.0	1.23	0.18	49.75	0.00	49.75	1.96	0.29	3.00×10^{-3}
AFO	100.0	1.03	0.15	59.13	0.00	59.13	2.51	0.28	1.88×10^{-3}
SAF	100.0	1.29	0.18	56.19	0.00	56.19	2.39	0.25	1.82×10^{-3}
EDI	16.2	2.74	0.36	106.06	35.70	141.75	1.53	0.19	8.90×10^{-4}
AEL	91.2	1.09	0.13	473.30	7.25	480.55	19.21	0.05	4.93×10^{-6}

References

[1] C. Baerlocher and L. B. McCusker, *Database of Zeolite Structures*, http://www.iza-structure.org/databases/, Online; accessed Jan. 1, 2010.

[2] R. Pophale, P. A. Cheeseman and M. W. Deem, *Phys. Chem. Chem. Phys.*, 2011, **13**, 12407.

[3] T. F. Willems, C. H. Rycroft, M. Kazi, J. C. Meza and M. Haranczyk, *Microporous Mesoporous Mater.*, 2012, **149**, 134–141.

[4] M. Pinheiro, R. L. Martin, C. H. Rycroft and M. Haranczyk, *CrystEngComm*, 2013, **15**, 7531–7538.

[5] D. Frenkel and B. Smit, *Understanding Molecular Simulation: From Algorithms to Applications*, Elsevier Science, 2002.

[6] A. L. Myers and J. M. Prausnitz, *AIChE J.*, 1965, **11**, 121–127.

[7] J. Kim, R. L. Martin, O. Rübel, M. Haranczyk and B. Smit, *J. Chem. Theory Comput.*, 2012, **8**, 1684–1693.

[8] J. Kim and B. Smit, *J. Chem. Theory Comput.*, 2012, **8**, 2336–2343.

[9] E. García-Pérez, J. B. Parra, C. O. Ania, A. García-Sánchez, J. M. van Baten, R. Krishna, D. Dubbeldam and S. Calero, *Adsorption*, 2007, **13**, 469–476.

[10] J. Kim, A. Maiti, L.-C. Lin, J. K. Stolaroff, B. Smit and R. D. Aines, *Nat. Commun.*, 2013, **4**, 1694.

[11] J. Kim, M. Abouelnasr, L.-C. Lin and B. Smit, *J. Am. Chem. Soc.*, 2013, **135**, 7545–7552.

[12] D. Peng and D. B. Robinson, *Ind. Eng. Chem. Fundamen.*, 1976, **15**, 59–64.

[13] O. Talu and A. L. Myers, *AIChE J.*, 2001, **47**, 1160–1168.

[14] E. Jones, T. Oliphant, P. Peterson *et al.*, *SciPy: Open source scientific tools for Python*, 2001–, http://www.scipy.org/, Online; accessed Apr. 8, 2015.

[15] H. Akima, *J. ACM*, 1970, **17**, 589–602.

[16] F. Pedregosa, G. Varoquaux, A. Gramfort, V. Michel, B. Thirion, O. Grisel, M. Blondel, P. Prettenhofer, R. Weiss, V. Dubourg, J. Vanderplas, A. Passos, D. Cournapeau, M. Brucher, M. Perrot and E. Duchesnay, *J. Mach. Learn. Res.*, 2011, **12**, 2825–2830.

[17] C. M. Simon, R. Mercado, S. K. Schnell, B. Smit and M. Haranczyk, *Chem. Mater.*, 2015, **27**, 4459–4475.

[18] E. Braun, A. F. Zurhelle, W. Thijssen, S. K. Schnell, L.-C. Lin, J. Kim, J. A. Thompson and B. Smit, *High-Throughput Computational Screening of Nanoporous Adsorbents for CO2 Capture from Natural Gas*, Open Science Framework, 2016, http://doi.org/10.17605/OSF.IO/KTBY4, Online.

[19] L. Breiman, J. Friedman, C. J. Stone and R. Olshen, *Classification and Regression Trees*, Chapman & Hall/CRC, 1984.

[20] Y. Bae and R. Q. Snurr, *Angew. Chem., Int. Ed.*, 2011, **50**, 11586–11596.